OFCDM SYSTEMS OVER FADING CHANNELS

BY

PENG LI

A Dissertation submitted to the Graduate School
in partial fulfillment of the requirements
for the Degree

Master of Applied Science

Concordia University
Montreal, Quebec, Canada, July 2009

Your file Votre référence
ISBN: 978-0-494-63030-3
Our file Notre référence
ISBN: 978-0-494-63030-3

ABSTRACT

OFCDM SYSTEMS OVER FADING CHANNELS

BY

PENG LI

Along with the fast growing demand of information exchange, telecommunication systems are required to provide fast and reliable service to high-data-rate applications such as video conference, real-time broadcasting, and on-line gaming. In downlink transmission, orthogonal frequency and code division multiplexing (OFCDM) has been an attractive technique for high-data-rate applications. With two-dimensional spreading, in both time domain and frequency domain, OFCDM achieves diversity gains in multiuser scenarios. Moreover, the adjustable spreading factors (SF) give OFCDM systems the flexibility in transmission rate and diversity gain.

In this thesis, we focus on the downlink of OFCDM communication systems. The performance of OFCDM systems is investigated over Ricean fading channels with Rayleigh fading as special case. Code division multiple access (CDMA) technique is used to support multiuser communications, where users can transmit at the same time using the same frequency with the help of code sequences. We compare different

combining methods that are employed to achieve diversity gain. Moreover, channel correlation is examined to see its effect on the system performance.

We also propose to combine multiple-input and multiple-output (MIMO) techniques, specifically space-time block coding (STBC), with OFCDM systems. By adding spatial diversity, a MIMO system can provide more reliable transmission compared to a single-input and single-output (SISO) system. The space-time scheme used in our study is Alamouti scheme [1], which employs $N = 2$ and M antennas at the transmitter side and receiver side respectively. In the thesis, we explain the system structure, transmission and detection methods, and system performance of such MIMO-OFCDM systems.

In our study, the expressions of system bit error rate (BER) are considered under the condition that no multi-code interference (MCI) is present. The accuracy of the BER expressions is verified when compared with the simulated ones for both SISO and MIMO-OFCDM systems with different combining methods. These comparisons are carried over different channels and with different system parameters to explore the benefits of OFCDM based systems. Both analytical and simulation results show the large diversity gains achieved when incorporating STBC with OFCDM.

ACKNOWLEDGMENTS

I would like to express my deepest appreciation to my supervisor, Dr. Walaa Hamouda. He is a great teacher. He focuses on his work and his students' success. He is a kind teacher who takes care of his students and tries his best to help his students. His guidance and encouragement is with every step of my research. Under his supervision, I am not only learning a lot of new concepts, but also learning how to gain new ideas and find out solutions, which will benefit myself in my future carrier. I would also like to thank my colleagues and friends who help me to complete this work in my graduate study. Finally, I would like to thank everyone at Concordia University. It is their hard working that makes Concordia a great University for students to pursue their academic education.

CONTENTS

LIST OF FIGURES

LIST OF ABBREVIATIONS

AWGN	.....	additive white Gaussian noise
BER	.....	bit error rate
BPSK	.....	binary phase-shift keying
CDMA	.....	code division multiple access
CSI	.....	channel state information
DAB	.....	digital audio broadcasting
DVB	.....	digital video broadcasting
DS-CDMA	.....	direct-sequence code division multiple access
EGC	.....	equal gain combining
FDMA	.....	frequency division multiple access
FFT	.....	fast Fourier transform
IFFT	.....	inverse fast Fourier transform
ICI	.....	intercarrier interference
ISI	.....	intersymbol interference
LOS	.....	line-of-sight

MAI	.....	multiple access interference
MC-CDMA	.....	multicarrier code division multiple access
MC-DS-CDMA	.....	multicarrier direct-sequence code division multiple access
MCI	.....	multi-code interference
MIMO	.....	multiple-input and multiple-output
MMSE	.....	minimum mean-square error
MRC	.....	maximal ratio combining
OFDM	.....	orthogonal frequency-division multiplexing
OFCDM	.....	orthogonal frequency and code division multiplexing
RV	.....	random variables
PAPR	.....	peak-to-average power ratio
PDF	.....	probability density function
OVSF	.....	orthogonal variable spreading factor
SC	.....	selection combining
SDMA	.....	space division multiple access
SF	.....	spreading factors
SISO	.....	single-input and single-output
SNR	.....	signal-to-noise ratio
SSMA	.....	spread spectrum multiple access
STBC	.....	space-time block coding

STTC	.....	space-time turbo coding
TDMA	.....	time division multiple access
WLAN	.....	Wireless Local Area Networks
WLL	.....	wireless local loop

LIST OF SYMBOLS

ζ	.....	system load
κ	.....	ratio of the dominant component to the total power of scattered waves in Ricean fading channel
μ_{h_1,h_2}	.....	correlation between channels h_1 and h_2
$\eta(l_i, j)$	.....	AWGN on the l_i-th sub-carrier during the j-th time slot
σ_I^2	.....	variance of AWGN that approximates MCI when $K_c >$ 50
σ_n^2	.....	variance of the noise added to each OFCDM symbol
$\widetilde{\rho}$	.....	ratio of total transmitted signal power for each symbol to the background noise power
C	.....	overall spreading code
C^F	.....	frequency domain spreading code

C^T	.....	time domain spreading code
d_k	.....	transmitted data symbol of the k-th user
$\widehat{d_k}$	.....	hard decision of the k-th user's data symbol
E_s	.....	transmitted signal energy
$\overrightarrow{e}$	.....	error vector between transmitted and received data symbol
K	.....	total number of spreading codes used
K_c	.....	number of interfering codes
h_{l_i}	.....	channel fading coefficient of the l_i-th sub-carrier
L	.....	total number of sub-carriers of one OFCDM frame
l_i	.....	index of the i-th sub-carrier transmitting the k-th user's symbols
M	.....	number of receive antennas
N	.....	number of transmit antennas
N_B	.....	number of data symbols spread with the same spreading code
N_F	.....	frequency domain spreading factor
N_S	.....	length of overall spreading code
N_T	.....	time domain spreading factor
n_0	.....	AWGN noise

$P_e\|_h$	.....	probability of bit error conditioned on the channel
$r_k(l_i)$	.....	output of the k-th user time domain despreader on the l_i-th sub-carrier
$w(l_i)$	.....	combining weight of the l_i-th sub-carrier
$\widetilde{Y}$	.....	transformed received signals
y_k	.....	output of the k-th user frequency domain despreader
z_k	.....	decision variable of the k-th user's data symbol

CHAPTER 1

INTRODUCTION

1.1 Introduction

In wireless communication systems, electromagnetic energy that is carrying data propagates from transmit antennas to receive antennas. Major problems raised in electromagnetic wave propagation are the multipath fading and multiple access interference (MAI). When the transmitted signal arrives at the receiver through different propagation paths with different delays, intersymbol interference may occur. Moreover, signals via different paths may be destructive due to phase difference, and this phenomenon is called signal fading. Reflection, diffraction, and scattering are three major mechanisms that cause multipath propagation [2]. Multiple-input and multiple-output (MIMO) techniques such as space-time trellis coding (STTC) and Space-time block coding (STBC) are introduced and widely studied to overcome the problem of fading through diversity [3][4]. MIMO techniques implement multiple transmit and receive antennas to transmit the same signal through independent channels to provide reliable wireless transmission. STTC and STBC are two different MIMO coding techniques used to achieve spatial diversity for reliable transmission [2].

Compared to a single-input and single-output (SISO) system, a MIMO system can support high-data-rate applications and improve received signal quality [5]. At the transmitter side, spatial diversity can be achieved by simple yet efficient STBC. The

first STBC introduced by Alamouti reaches full transmit diversity with two transmit antennas [1].

In a transmission system where the transmitted signal experiences multipath fading and noise degradation, a combining technique is needed to identify and combine the components from the same transmitted signal. These combining techniques can generally be grouped into selection combining (SC), gain combining, and hybrid selection/gain combining [5]. In selection combining, the received signal from the transmission path with the highest signal-to-noise ratio (SNR) is selected for detection. However in gain combining, signals from all transmission paths are combined to detect the transmitted data. Some typical gain combining techniques are maximal ratio combining (MRC), equal gain combining (EGC), and minimum mean-square error (MMSE) combining.

System bandwidth, transmission rate, and error probability are three main characteristics in evaluating wireless communication systems. To optimize the use of available bandwidth is one of the major topics in the study of wireless communication systems. Multiple-access systems provide a solution for optimizing frequency use and maximizing flexibility. For instance, frequency-division multiple access (FDMA), time-division multiple access (TDMA), spread spectrum multiple access (SSMA), and space-division multiple access (SDMA) are well investigated and implemented in different communication systems [6]. Also, orthogonal frequency-division multiplexing (OFDM) is one useful multiplexing scheme that has attracted many researchers [7]. It divides data into a set of parallel streams to be transmitted using mutually orthogonal frequency bands. Because of this orthogonality, the data streams can be

transmitted at the same time to increase the system transmission rate. On the other hand, CDMA is one form of "spread-spectrum" signaling [8] that is broadly used in telecommunication systems. In a CDMA system, users are assigned orthogonal codes so that different users can share the same frequency band at the same time with little or no interference. One integration of OFDM and CDMA techniques, called OFCDM, takes advantage of both OFDM and CDMA systems to gain frequency diversity and achieve high but flexible transmission rates [9].

With two-dimensional spreading, OFCDM is an attractive transmission technique for high-data-rate applications. In OFCDM, spreading in frequency domain provides frequency diversity gain. On the other hand, a large time domain spreading factor allows more users to access the system at the same time, whereas a small time domain spreading factor is more suitable for high-data-rate applications [9]. Combined with MIMO technology, a MIMO-OFCDM system can provide high reliability with flexible transmission rates. We can therefore expect a great potential from MIMO-OFCDM systems. Recently, many studies have been carried out for OFCDM systems on how to gain frequency domain diversity and on the effect of multi-code interference (MCI) on achieving this diversity [9]-[12]. In [9], the authors presented the system structure of SISO-OFCDM. They also explained the detection method using MMSE combining and iterative MCI cancellation scheme. In [13], the authors briefly mention the MIMO-OFCDM system structure. However, the system performance in terms of BER under different fading channels has not been addressed. Therefore, this thesis focuses on the system performance of OFCDM systems over slow fading channels. Semi-analytical results of BER are obtained for both SISO and MIMO-OFCDM sys-

tems using different combining techniques. We also explain the system structures and detection methods for both SISO-OFCDM and MIMO-OFCDM systems in detail.

1.2 Thesis Contribution

The major contributions of this thesis are listed as follows:

1. The study of OFCDM systems, including the system structure, transmission techniques involved, and detection methods. OFCDM systems over Rayleigh fading and Ricean fading channels with MRC, EGC, and MMSE combining are investigated.

2. We illustrate how to extend SISO-OFCDM systems to MIMO-OFCDM systems by adding spatial diversity. In MIMO-OFCDM systems, we employ Alamouti scheme to achieve transmit diversity of $N = 2$ and use MRC, EGC, and MMSE combining to obtain receive diversity M, where M is the number of receive antennas.

3. We present semi-analytical results for the BER of both SISO-OFCDM and MIMO-OFCDM systems over fading channels. The results obtained are applicable for OFCDM systems over any channel model.

1.3 Thesis Outline

The contents of this thesis are outlined as follows:

In Chapter 2, we give a review of some background of major concepts involved in this thesis. We present OFDM, CDMA, and OFCDM communication techniques.

Finally, we review some commonly used detection methods.

Chapter 3 focuses on SISO-OFCDM systems with two dimensional spreading over slow fading channels. MRC, EGC, and MMSE combining techniques used at the receiver are studied. The performance of different multiuser scenarios is investigated where the BER is analyzed. We also derive closed-form semi-analytical expressions for the BER in systems with different combining techniques.

In Chapter 4, we extend the results in Chapter 3 to MIMO-OFCDM systems when using STBC. For M receive antennas, gain combining techniques are used to extract receive diversity. The same as SISO-OFCDM systems, the performance of different combining schemes are studied for multiuser scenarios. BER semi-analytical results are then presented.

In Chapter 5 we present our conclusions and possible future directions in this area.

CHAPTER 2

BACKGROUNDS

In this chapter, we explain some key concepts related to the work in this thesis. These concepts include multipath fading, transmission techniques including OFDM, CDMA, and STBC, detection and combining methods such as MRC, EGC, and MMSE.

2.1 Multipath Fading

In wireless communication systems, the physical path from transmit antennas to receive antennas is not always a straight line of sight but subject to multipath propagation [2]. Each copy of the original electromagnetic wave goes through a unique propagation path, and along these paths signals may arrive at the receiver side at different times with different attenuation and different phase. Thus, the overall received signal may be constructive or destructive causing signal fading.

Multipath fading channels can be grouped into frequency flat-fading channels and frequency-selective fading channels. In flat-fading channels, the coherence bandwidth of the channel is larger than the signal bandwidth, and the signal on all frequency bands will experience the same fading amplitude. However, in frequency-selective fading channels, the bandwidth of the channel is smaller than the signal bandwidth, and different frequency components of the same signal may experience different fading amplitudes [14].

Because of the uniqueness of each multipath fading channel, some representative channel models are used for study and research. Two commonly used fading channel models are Rayleigh fading and Ricean fading channels.

2.1.1 Rayleigh Fading

Rayleigh fading model is used to characterize physical channels with large amount of randomly moving scattered signal components received by the receive antennas. When the scattering mechanism dominates the electromagnetic wave propagation, the channel fading coefficient follows a Rayleigh distribution. It is known that Rayleigh distribution is closely related to central chi-square distribution. Suppose we have two independent Gaussian distributed random variables (RV) X_1 and X_2, each with zero-mean and variance σ^2. Then the RV $Y = X_1^2 + X_2^2$ follows chi-square distribution with two degrees of freedom. Let us define a RV $R = \sqrt{Y} = \sqrt{X_1^2 + X_2^2}$. Thus, the distribution of R is said to have a Rayleigh distribution [14].

The probability density function (PDF) can be derived from the PDF of chi-square distributed RV Y to give [14]

$$p_{Rayleigh}(r) = \frac{r}{\sigma^2} \cdot e^{(-\frac{r^2}{2\sigma^2})}, \quad r \geq 0. \tag{2.1}$$

From (2.1) we can see that the Rayleigh PDF is characterized by σ^2, the variance at each dimension. Let us define $\Omega = \sigma^2$, the PDF of the Rayleigh RV is shown in Figure 2.1 for different values of Ω.

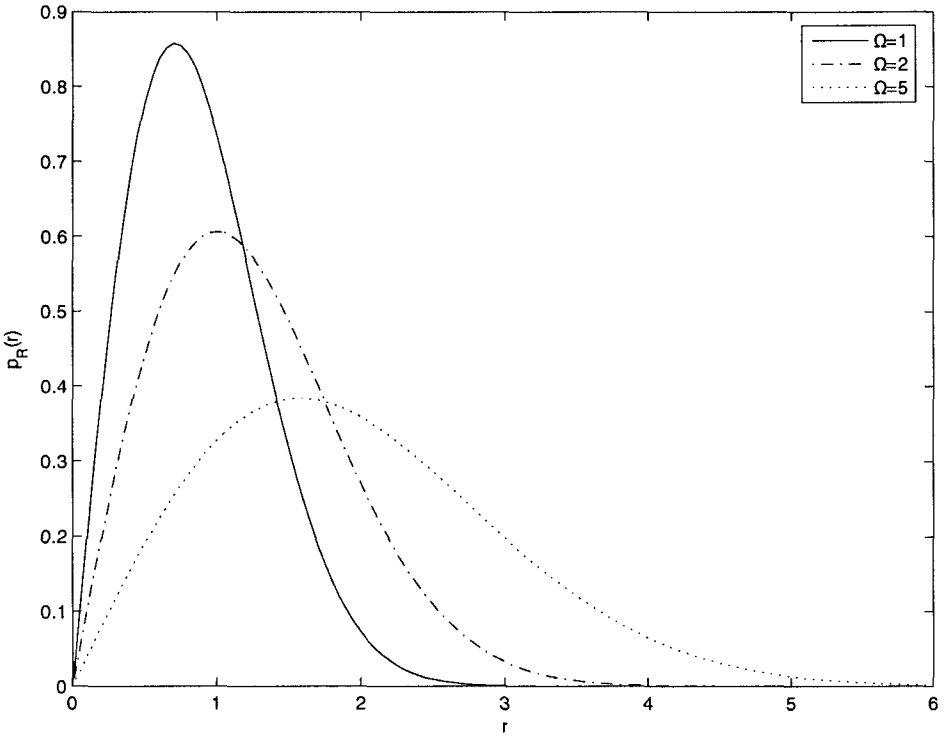

Figure 2.1: PDF of Rayleigh distribution with different Ω

2.1.2 Ricean Fading

In some cases, besides the scattering paths, there exists a straight path from the transmitter to the receiver, known as line-of-sight (LOS). When the presence of LOS cannot be ignored, Ricean fading is more suitable for modeling these channels. In this case, the Ricean fading channel model is a summation of LOS and Rayleigh distributed scattered components. Different from Rayleigh distribution, the Ricean distribution is closely related to noncentral chi-square distribution [14].

Suppose we have two independent Gaussian distributed RVs X_1 and X_2 with non-zero means m_1 and m_2 respectively, and variance σ^2. Then, the RV $Y = X_1^2 + X_2^2$ follows noncentral chi-square distribution with two degrees of freedom. Similar to the

Rayleigh distribution, let us define a RV $R = \sqrt{Y} = \sqrt{X_1^2 + X_2^2}$, then the distribution of R is defined as a Ricean distribution. The relationship between the noncentrality parameter s of the Ricean distribution and the mean of X_1 and X_2 is [14]

$$s^2 = m_1^2 + m_2^2. \tag{2.2}$$

The PDF of the Ricean RV can be derived from the PDF of noncentral chi-square distributed RV Y, to give [14]

$$p_{Ricean}(r) = \frac{r}{\sigma^2} \cdot e^{(-\frac{r^2+s^2}{2\sigma^2})} \cdot I_0(\frac{rs}{\sigma^2}), \ \ r \geq 0. \tag{2.3}$$

In (2.3), I_0 is the 0-th order modified Bessel function of the first kind.

The PDF of the Ricean distribution is characterized by the ratio of the dominant component and the total power of scattered waves. We can denote this ratio by κ, and for the normalized envelope, the Ricean PDF is given by [15]

$$p_{Ricean}(r) = \frac{2(1+\kappa)}{e^{\kappa+(1+\kappa)r^2}} \cdot r \cdot I_0(2r \cdot \sqrt{\kappa(1+\kappa)}). \tag{2.4}$$

The PDF of Ricean RV with different values of κ is shown in Figure 2.2. From (2.3) we can see that when $\kappa = 0$, the Ricean distribution reduces to the Rayleigh distribution.

2.1.3 Channel Correlation

In wireless communication systems, different channels may have certain degrees of similarity, known as channel correlation. Suppose we have two channels h_1, h_2, and we take L samples from each channel marked as s_l^1 and s_l^2, where $l = 1, 2, ...L$. When

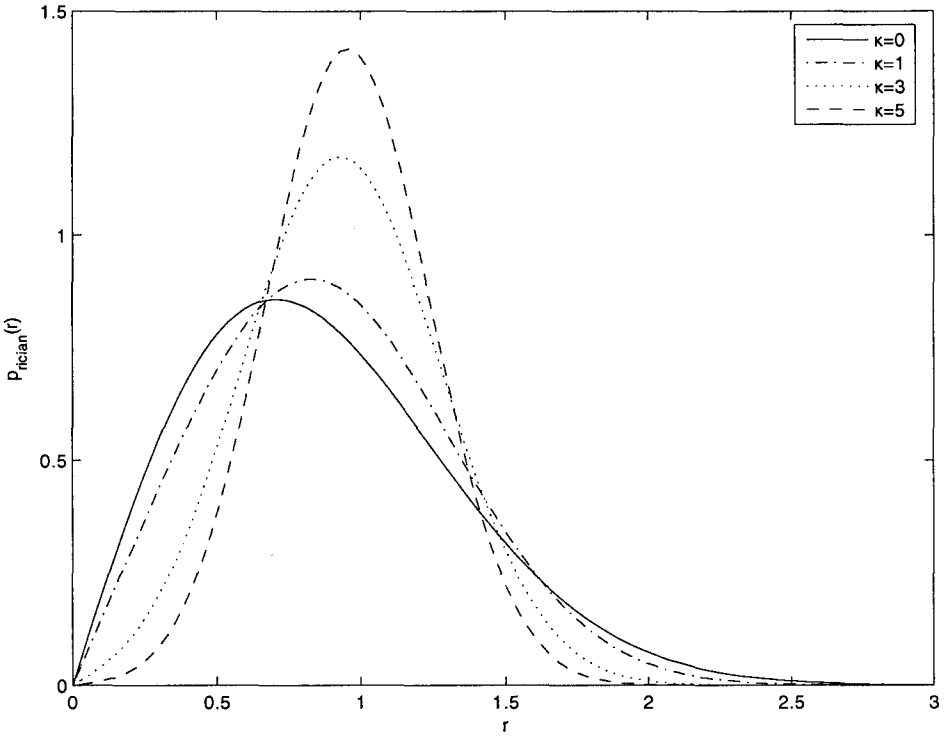

Figure 2.2: PDF of Ricean distribution with different κ

the variance of the channel distributions are $\sigma_{h_1}^2$ and $\sigma_{h_2}^2$, and the mean values are $\overline{m_{h_1}}$ and $\overline{m_{h_2}}$ respectively, the correlation between these two channels is given by [7]

$$\mu_{h_1,h_2} = \frac{\sum_{l=1}^{L}(s_l^1 - \overline{m_{h_1}})(s_l^2 - \overline{m_{h_2}})}{(L-1)\sigma_{h_1}\sigma_{h_2}}. \tag{2.5}$$

Spatial channels can have correlation, and sub-carriers in the same OFDM system may also have correlation. In an OFCDM system, each transmitted data spreads in frequency domain to obtain frequency diversity gain. In order to achieve maximum frequency diversity, all the sub-carriers dedicated to the same transmitted data have to be mutually independent. If sub-carriers are correlated, the frequency diversity will

be reduced and the BER performance will be degraded. In most cases presented in this thesis, we assume to use ideal interleavers to maximize the frequency diversity, where all the sub-carriers are independent. However, we will also show the BER performance degradation due to correlation in Rayleigh fading channels. The unit power correlated Rayleigh fading channels, denoted as h_1 and h_2, with given correlation coefficient can be generated according to the scheme introduced in [16]. The steps are briefly given below [16]:

1. For a given correlation, μ_{h_1,h_2}, find the root λ, $0 \leq \lambda \leq 1$, of the empirical equation

$$0.2155\lambda^3 + 0.7352\lambda^2 + 0.0465\lambda - 0.0026 - \mu_{h_1,h_2} = 0. \tag{2.6}$$

2. Generate two unit power uncorrelated Rayleigh fading signals, ω_1 and ω_2.

3. Calculate the coloring matrix $\mathbf{L}$ by

$$\mathbf{L} = \begin{bmatrix} 1 & 0 \\ \frac{\lambda(1+i)}{\sqrt{2}} & \sqrt{1-\lambda^2} \end{bmatrix}, \tag{2.7}$$

   where i is the square root of -1.

4. Calculate $\mathbf{X}$ by

$$\mathbf{X} = \mathbf{L} \cdot \begin{bmatrix} \omega_1 \\ \omega_2 \end{bmatrix} = \begin{bmatrix} x_1 \\ x_2 \end{bmatrix}. \tag{2.8}$$

5. x_1 and x_2 are the desired Rayleigh fading channel coefficients.

Figure 2.3 shows Rayleigh fading envelopes with channel correlation coefficient equals to 0.95 and 0.05 respectively. In our work when correlation is considered, the

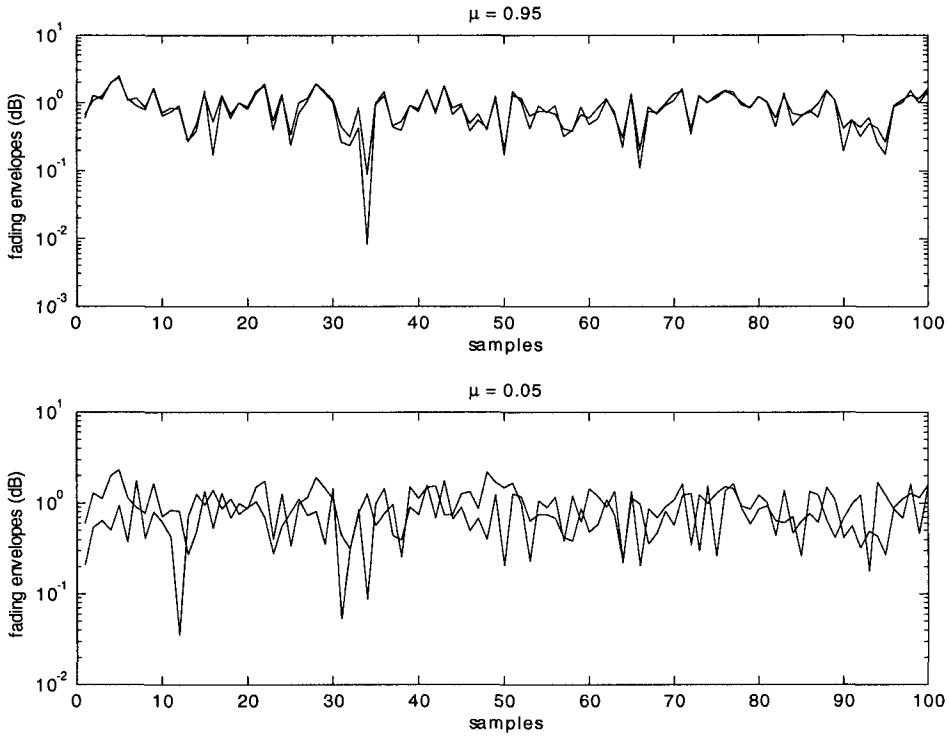

Figure 2.3: Correlated Rayleigh fading envelopes

correlated Rayleigh fading channels are generated according to the scheme described above.

2.2 OFDM

As the name suggests, OFDM system employs a number of orthogonal frequencies to transmit signals. In OFDM systems, user data is split into streams and loaded onto mutually orthogonal sub-carriers that are then multiplexed to generate an OFDM symbol for transmission [6]. The key feature is the orthogonality in frequency domain among those sub-carriers. Suppose we have a base sub-carrier with frequency f and period T, where $f = 1/T$, then the frequency of each sub-carrier in the OFDM

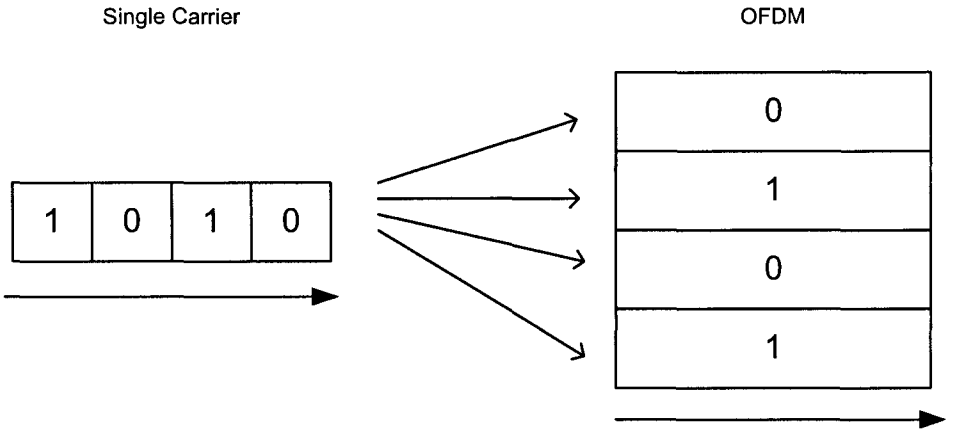

Figure 2.4: Using OFDM to extend data symbol duration

system is equal to f multiplied by a unique positive integer k. Let m and n be two different positive integers, then mf and nf can represent two different sub-carriers in the OFDM system. Because of the orthogonality, the sub-carriers carrying data in an OFDM system can be multiplexed together to transmit simultaneously. At the receiver side, matched filters corresponding to each sub-carrier are used to demultiplex and extract the data.

One advantage of OFDM systems is that it can minimize intersymbol interference (ISI). As suggested in Figure 2.4, compared to single carrier systems, an OFDM system extends the data symbol duration by allowing a data stream to transmit in parallel; therefore, ISI is reduced. Another advantage is that OFDM can increase the transmission rate, which is more suitable for high-data-rate applications. From Figure 2.5 we can see that by allowing data streams to transmit in parallel, an OFDM system takes a small fraction of time to transmit the same amount of data compared to a single carrier system. The third advantage is that OFDM helps to handle severe

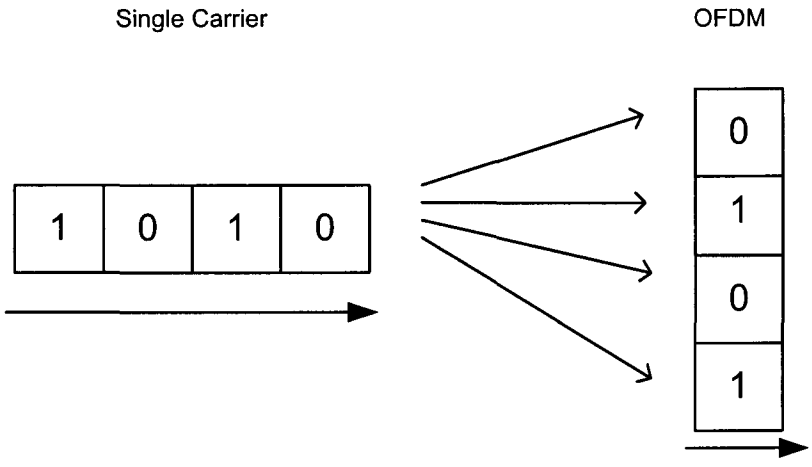

Figure 2.5: Using OFDM to increase transmission rate

channel fading and reduce outage probability [17]. This can be explained as follows. In a communication system, some frequency bands may encounter severe interference or fading. If all data is transmitted through those deteriorated frequency bands, outage will occur. However, an OFDM system employs different frequency bands to transmit the data from the same user. Even if one or few sub-carriers encounter sever fading, the whole OFDM system can still maintain a reasonable performance.

In OFDM systems, the serial data is split into parallel streams and mapped onto different, mutually orthogonal sub-carriers. Then by inverse fast Fourier transform (IFFT) operation, the frequency domain signal is converted into time domain for transmission. Orthogonality is the key characteristic of OFDM technique. However, the physical channel in time domain may have variations during one OFDM frame, which destroys the orthogonality and power leakage among sub-carriers. This effect is known as intercarrier interference (ICI) [18]. In [19], some techniques are presented to

reduce ICI. Another disadvantage of OFDM is that it has high peak-to-average power ratio (PAPR). Many profound studies have been carried out, and different solutions of peak-to-average power control are proposed for both SISO and MIMO-OFDM systems [20]-[24].

During time domain transmission of OFDM system, ISI may occur due to multi-path delays. ISI can be mitigated by inserting guard intervals (a redundant symbol extension) between transmitted sequences [6]. However, inserting guard intervals causes deduction in transmission efficiency. In [25] and [26], the authors proposed coding techniques for OFDM systems to restore the transmission efficiency without sacrificing system performance.

After experiencing channel fading and noise, the received time domain signal is converted back into frequency domain by fast Fourier transform (FFT) [6][17]. Matched filters are then used to extract the data streams from each sub-carrier. Those received parallel data streams are converted back to serial data and then used for detection.

Because of the advantages of OFDM, many high-speed wireless transmission schemes such as MC-CDMA and OFCDM are based on OFDM technique [9][27][28]. New studies mainly focus on MIMO-OFDM systems that are more suitable for high-data-rate applications than traditional OFDM systems [29]-[32].

2.3 CDMA

Similar to OFDM, which uses orthogonal frequencies to transmit data at the same time, CDMA uses orthogonal codes to transmit data using the same frequency

at the same time. Now, CDMA becomes a widely used channel multiple access method that allows multiple users to access the channel at the same time. In a basic CDMA system, the data from each user is assigned a unique code, which is also called signature waveform. For a length-L code, C_k, where $C_k = \begin{bmatrix} c_0^k & c_1^k & ... & c_{L-1}^k \end{bmatrix}$, the component c_l^k $(l = 0, 1, ..., L-1)$ is called a chip [14]. The most important property of the codes is due to its orthogonality. Suppose we have two length-L codes C_i and C_j $(i \neq j)$ assigned to two different users. The orthogonality implies that

$$C_i C_j^{\mathbf{T}} = \sum_{l=0}^{L-1} c_l^i \cdot c_l^j = 0, \tag{2.9}$$

where $(\cdot)^{\mathbf{T}}$ represents transpose operation.

Because of the orthogonality, the implementation of CDMA is simple. At the transmitter side, each user's data is spread by multiplying a unique code from a code set [14]. Then, the spread signals from different users are multiplexed and transmitted at the same time. The received signal at the receiver side is given by

$$r = \sum_{k=0}^{K-1} \sqrt{E_s} \cdot h \cdot d_k \cdot C_k + n_0, \tag{2.10}$$

where K is the number of users, E_s is the transmitted signal energy for each symbol, h is the channel coefficient, d_k is the transmitted data for the k-th user, C_k is the unique code assigned to the k-th user, and n_0 is the additive white Gaussian noise (AWGN). Here we assume all users' signals are synchronized during transmission, and we keep this assumption throughout the thesis. At the receiver side, the received signal is applied to a filter matched to the user's code followed by a decision to recover the transmitted data.

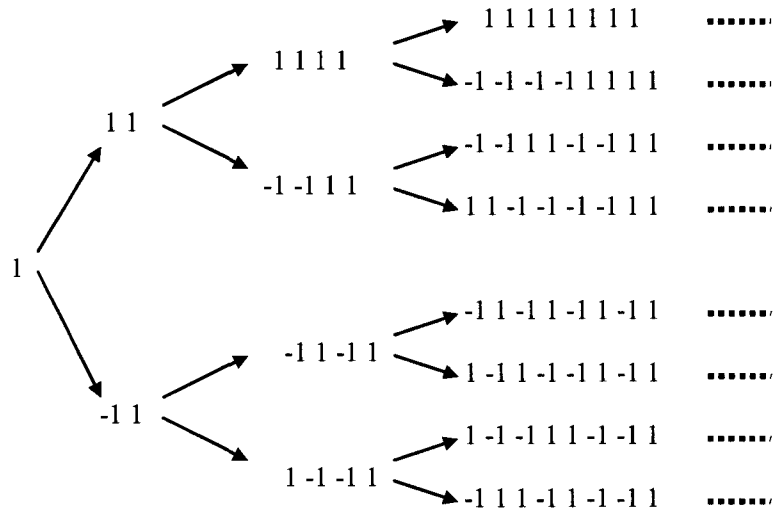

Figure 2.6: OVSF code generation

One common spreading technique is direct-sequence code division multiple access (DS-CDMA). A DS-CDMA signal is generated by direct multiplication of user data by its code sequence [33]. Spread by orthogonal codes, data from different users can be multiplexed and transmitted at the same time. At the receiver side, the received data is applied to a bank of matched filters to recover each user data.

By using orthogonal codes, CDMA system can support multi-user scenario and can provide flexible transmission rate by varying the length of the spreading codes [34][35]. Nowadays, this multi-user transmission scheme is combined with MIMO technology to provide reliable service for both uplink and downlink transmission [36]-[39].

2.4 Orthogonal Variable Spreading Factor

Orthogonal variable spreading factor (OVSF) is a simple technique used to generate orthogonal codes for CDMA systems. Figure 2.6 shows how OVSF codes are generated by using a complete binary tree. Depending on the level in the tree where an OVSF code is located, the spreading factor of the OVSF code is determined. An OVSF code can be assigned to a user if and only if the code and all of its ancestor OVSF codes and descendant OVSF codes in the tree have not been assigned to other users. Once the level (length) of the OVSF code is chosen, the total data rate that can be assigned to users is fixed [40]. Hence, an OVSF code with small SF is ideal for high-data-rate applications.

2.5 MC-CDMA

One combination of OFDM with CDMA techniques is MC-CDMA. Basic concepts of MC-CDMA can be found in [41] and [42]. In brief, MC-CDMA system spread each symbol by a unique spreading code, then transmit spread symbols with an OFDM system.

According to [41], MC-CDMA can be categorized into two groups. One group spreads data symbols in frequency domain, then the spread replicas of the same symbol are combined to recover the transmitted symbol. Normally, MC-CDMA refers to this group. Another group spreads data symbols in time domain to form data streams. Then different streams are transmitted in parallel in an OFDM system. This MC-CDMA scheme is also called multicarrier direct-sequence code division multiple

access (MC-DS-CDMA) [43]. Frame structures of MC-CDMA and MC-DS-CDMA are compared in Figure 2.7.

MC-CDMA has the same drawbacks as OFDM since it employs OFDM system to transmit data symbols. However, by implementing CDMA scheme to multiplex different symbols, MC-CDMA system can lower the symbol rate in each sub-carrier. Thus, symbol duration is enlarged, which makes it easier to quasi-synchronize the transmissions [41].

With the advantages offered by MIMO technology, the combination of MIMO and MC-CDMA is widely studied to exploit the benefits of MC-CDMA in multi-user scenarios [44]-[46]. For instance, [44] presents an example of MIMO-MC-CDMA system using STBC, and [46] explains how to implement space-time coding and spatial multiplexing to benefit from both spatial diversity and at the same time improve spectral efficiency.

2.6 OFCDM

Another integration of OFDM and CDMA is called OFCDM. Typical implementation of CDMA into OFDM-based system includes MC-DS-CDMA, MC-CDMA, and OFCDM. Figure 2.7 presents the difference among these three schemes. MC-DS-CDMA systems spread symbols in time domain only, so they cannot achieve frequency domain diversity. On the other hand, MC-CDMA systems spread symbols in frequency domain only, so they cannot adapt to variable transmission rates. In an OFCDM system, symbols are spread in both frequency and time domain. Therefore, OFCDM systems can deliver frequency diversity gain and can be adapted to appli-

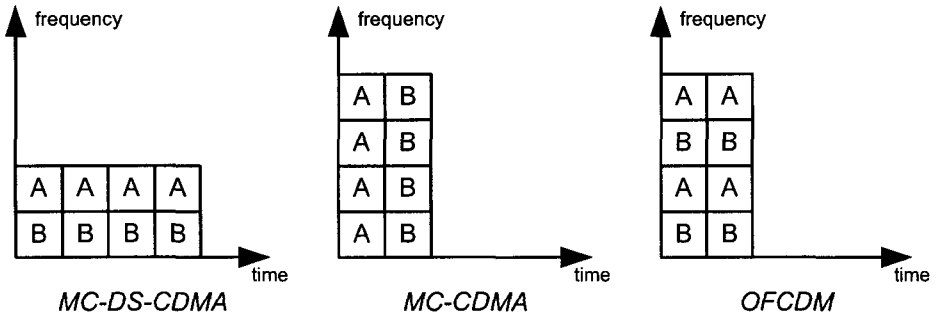

Figure 2.7: Different spreading schemes in multicarrier systems

cations with different transmission rates, which is preferred in the 4G transmission systems [28][47].

In frequency-selective channels, signal transmitted on some sub-carriers may experience deep fade or outage. Therefore, if the spreading factors are too small, the OFCDM system cannot fully benefit from the multipath diversity. On the other hand, based on the OVSF code assignment criteria, when assigning the OVSF code with a large spreading factor to a user may preclude a larger number of OVSF codes with small spreading factors [40]. Therefore, the length of spreading codes in frequency domain and time domain should be properly chosen to satisfy the system requirements.

In the frequency domain, the sub-carriers of an OFDM system are expected to experience different fading and hence the orthogonality is no longer preserved. Therefore, at the receiver side, a combining technique is employed for de-spreading. In these OFCDM systems, gain combining methods such as MRC, EGC, and MMSE combin-

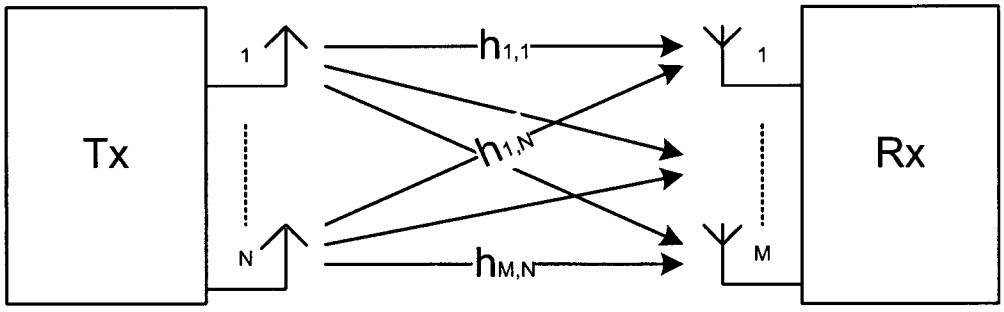

Figure 2.8: MIMO system model

ing are preferable to extract the original data from the received OFCDM symbols.

2.7 MIMO Systems

Nowadays, there is a rapid growth in the demand of high-speed and reliable wireless communication services. Increasing the diversity in the frequency domain might be a solution. However in reality, the frequency spectrum is limited and shared by different users, whose number is also increasing rapidly. On the other hand, high-speed applications put strong constrain on transmission time, which restricts the time domain diversity within certain degree. Moreover, spatial diversity has attracted research attention since it can help to adapt high-speed applications in multipath environments. Spatial diversity is achieved by implementing suitable transmitting and receiving schemes with multiple transmit and multiple receive antennas, known MIMO systems. Compared to SISO systems, MIMO systems support higher data rates with better reliability. Therefore, MIMO technology has already been included in the 4G standards [28][48].

Figure 2.8 presents a brief structure of a MIMO system. At the transmitter

side, data is transmitted from N transmit antennas according to some transmission technique. After transmission through different channels, M receive antennas pick up the signals which are then sent for detection. The channel matrix of a MIMO system is defined as $N \times M$ matrix $\mathbf{H}$:

$$\mathbf{H} = \begin{bmatrix} h_{1,1} & h_{2,1} & ... & h_{M,1} \\ h_{1,2} & h_{2,2} & ... & h_{M,2} \\ ... & ... & ... & ... \\ h_{1,N} & h_{2,N} & ... & h_{M,N} \end{bmatrix}. \tag{2.11}$$

The element $h_{i,j}$ $(i = 1, 2, ..., M,\ j = 1, 2, ..., N)$ represents the fading coefficient corresponding to the link from the j-th transmit antenna to the i-th receive antenna. When all channel coefficients are independent, maximum spatial diversity of $N \times M$ is obtained. To achieve this maximum spatial diversity, the antenna spacing should be adjusted to be much larger than the transmitted signal wavelength [14]. If the antennas at either transmitter side or receiver side are not well physically separated, correlation between channels will degrade the system performance [5].

In a MIMO system, user data, d_0, is first spread over the N transmit antennas according to a transmit scheme to achieve transmit diversity gain [2][5]. Normally the transmitter side has no knowledge of the channel state information (CSI), hence the transmitted power is equally allocated to all transmit antennas. At the receiver side, the received signal picked up by the i-th receive antenna is given by

$$r_i = \sum_{i=1}^{N} \sqrt{\frac{E_s}{N}} \cdot d_{0,j} \cdot h_{i,j} + n_i, \tag{2.12}$$

where E_s is the total transmitted energy for d_0, $d_{0,j}$ is the user data spread on the

j-th transmit antenna according to the selected space-time coding scheme, and n_i is the AWGN at the i-th receiver antenna. We can also represent the MIMO system in matrix form as:

$$\mathbf{r} = \sqrt{\frac{E_s}{N}} \cdot \mathbf{d}_0 \cdot \mathbf{H} + \mathbf{n}, \tag{2.13}$$

where

$$\mathbf{r} = \begin{bmatrix} r_1 & r_2 & \dots & r_M \end{bmatrix}, \tag{2.14}$$

$$\mathbf{d}_0 = \begin{bmatrix} d_{0,1} & d_{0,2} & \dots & d_{0,N} \end{bmatrix}, \tag{2.15}$$

$$\mathbf{n} = \begin{bmatrix} n_1 & n_2 & \dots & n_M \end{bmatrix}. \tag{2.16}$$

In MIMO systems, maximum likelihood detection can be used at the receiver side to give data estimates [2]:

$$\widehat{d_0} = \arg\min_{d_0} \sum_{i=1}^{M} \left| r_i - \sum_{j=1}^{N} \sqrt{\frac{E_s}{N}} \cdot d_{0,j} \cdot h_{i,j} \right|^2. \tag{2.17}$$

2.7.1 STTC

First introduced in [3], STTC transmits multiple copies of each data symbol during different time slots over different transmit antennas so that to achieve diversity. As suggested by its name, the transmit scheme of STTC is based on trellis coding. Figure 2.9 presents an example STTC encoding method for QPSK symbols using two transmit antennas. Normally the encoder is initialized to state S_0. At each step of the trellis, when current state is S_a ($a = 0, 1, 2, 3$) and the input is b ($b = 0, 1, 2, 3$), the encoder output is $\begin{bmatrix} a & b \end{bmatrix}$. The two symbols of the encoder output are mapped to the two transmit antennas respectively for transmission. Then the encoder changes to state S_b according to the four-state code trellis and starts next step of encoding.

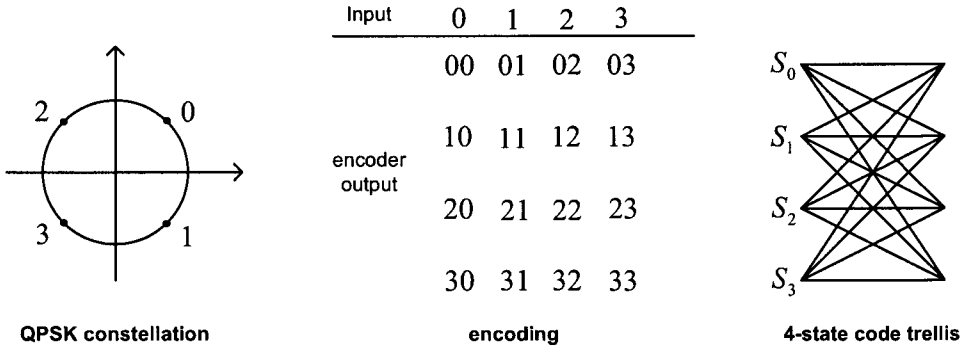

Figure 2.9: A four-state QPSK STTC

In a general MIMO system with N transmit antennas and M receive antennas, the received signal at the m-th ($m = 1, 2, ..., M$) receive antenna is given by

$$y_m(t) = \sqrt{E_s} \sum_{n=1}^{N} h_{m,n} x_n(t) + \eta_m(t), \tag{2.18}$$

where t represents the time slot, $h_{m,n}$ is the channel fading coefficient from the n-th transmit antenna to the m-th receive antenna, $x_n(t)$ is the encoded symbol transmitted from the n-th transmit antenna during t, and $\eta_m(t)$ represents the noise added to the m-th receive antenna during t. Then, the decoding of STTC is based on Viterbi algorithm [2][3].

Since STTC is based on trellis code, it can provide coding gain on top of the diversity gain. By using more complex decoder, STTC may deliver better BER performance than STBC introduced in the next section.

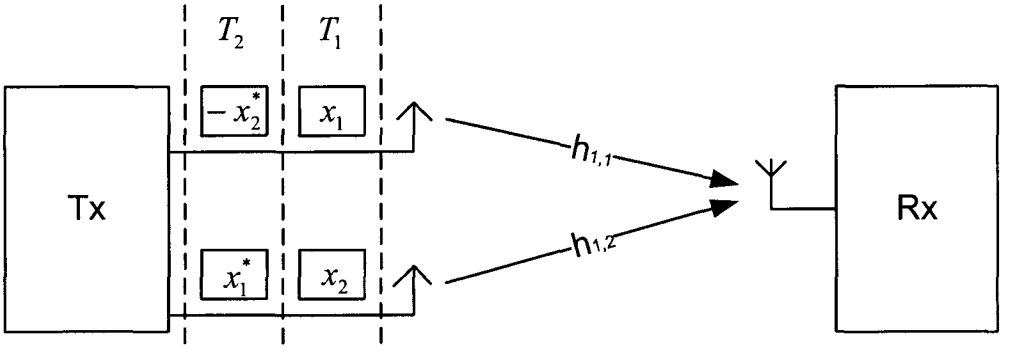

Figure 2.10: the Alamouti scheme

2.7.2 STBC

In some cases, receive diversity is hard to achieve. For example, the receive antennas in a mobile phone may not be separated far enough to pick up signals through independent paths [5]. Therefore, transmit diversity becomes crucial in order to achieve spatial diversity. STBC can help to achieve transmit diversity in a simple way. With STBC, a MIMO system transmits multiple copies of the same data across different transmit antennas during different time slots. At the receiver side, the received signals from different receive antennas are combined through a linear process to extract the signal for detection [2]. The simplest STBC scheme was introduced by Alamouti [1], which exploits full transmit diversity with two transmit antennas [2]. A system using Alamouti scheme with one receive antenna is show in Figure 2.10.

In Alamouti scheme, two symbols are transmitted at the same time from two different transmit antennas. It takes two time slots to transmit two symbols, so Alamouti scheme is full rate. Suppose user data x_1 and x_2 will be transmitted according to Alamouti scheme. During the first time slot, T_1, x_1 is transmitted from

the first transmit antenna and x_2 is transmitted from the second transmit antenna. During the second time slot, T_2, $-x_2^*$ is transmitted from the first transmit antenna and x_1^* is transmitted from the second transmit antenna, where $(\cdot)^*$ represent complex conjugate operation.

At the receiver side, the received signal for the two consecutive time slots is given by

$$y_{T_1} = \sqrt{\frac{E_s}{2}}\left(h_{1,1} \cdot x_1 + h_{2,1} \cdot x_2\right) + n_1 \tag{2.19}$$

$$y_{T_2} = \sqrt{\frac{E_s}{2}}\left(-h_{1,1} \cdot x_2^* + h_{2,1} \cdot x_1^*\right) + n_2, \tag{2.20}$$

where n_1 and n_2 are AWGN samples. One important assumption is that channel coefficients should be fixed during the two consecutive time slots.

Assuming the receiver side has perfect knowledge of the channel state information, the maximum likelihood estimates are [2]

$$\widehat{x}_1 = \arg\max_{x_1} P\left(x_1 \left| y_{T_1}, y_{T_2}, h_{1,1}, h_{2,1}\right.\right) \tag{2.21}$$

$$\widehat{x}_2 = \arg\max_{x_2} P\left(x_2 \left| y_{T_1}, y_{T_2}, h_{1,1}, h_{2,1}\right.\right). \tag{2.22}$$

By simple conversion, and according to Bayes' rule, the optimal decoding can be written as

$$\widehat{x}_1 = \arg\max_{x_1} P\left(h_{1,1}^* y_{T_1} + h_{1,2} y_{T_2}^* \left| x_1, h_{1,1}, h_{2,1}\right.\right) \tag{2.23}$$

$$\widehat{x}_2 = \arg\max_{x_2} P\left(h_{1,2}^* y_{T_1} - h_{1,1} y_{T_2}^* \left| x_2, h_{1,1}, h_{2,1}\right.\right). \tag{2.24}$$

Therefore, with different combination of y_{T_1} and y_{T_1}, the detector can decouple x_1 and x_2 to give [2]:

$$\widehat{x}_1 = \arg\min_{x_1} \left| h_{1,1}^* y_{T_1} + h_{2,1} y_{T_2}^* - \sqrt{\frac{E_s}{2}}(|h_{1,1}|^2 + |h_{2,1}|^2) \cdot x_1 \right| \tag{2.25}$$

$$\widehat{x}_2 = \arg\min_{x_2} \left| h_{2,1}^* y_{T_1} - h_{1,1} y_{T_2}^* - \sqrt{\frac{E_s}{2}}(|h_{1,1}|^2 + |h_{2,1}|^2) \cdot x_2 \right|. \tag{2.26}$$

For a system with M receive antennas, the optimal decision rule is given by [2]:

$$\widehat{x}_1 = \arg\min_{x_1} \left| \sum_{j=1}^{M} \left[h_{1,j}^* y_{T_1}(j) + h_{2,i} y_{T_2}^*(j) - \sqrt{\frac{E_s}{2}}(|h_{1,j}|^2 + |h_{2,j}|^2) \cdot x_1 \right] \right|^2 \tag{2.27}$$

$$\widehat{x}_2 = \arg\min_{x_2} \left| \sum_{j=1}^{M} \left[h_{2,j}^* y_{T_1}(j) - h_{1,j} y_{T_2}^*(j) - \sqrt{\frac{E_s}{2}}(|h_{1,j}|^2 + |h_{2,j}|^2) \cdot x_2 \right] \right|^2, \tag{2.28}$$

where $y_{T_1}(i)$ and $y_{T_2}(i)$ represent the received signal at the i-th receive antenna during the first and second time slots, respectively.

Let us denote ρ as the ratio of the transmitted signal power to the noise power, then ρ is given by

$$\rho = \frac{E_s}{2N_0}, \tag{2.29}$$

where E_s is the transmitted signal energy for each symbol during T_1 and T_2, and N_0 is the two-sided noise spectral density of n_1 and n_2. Using Alamouti scheme with M receive antennas, the BER is given by [2]

$$P_b = \left[\frac{1}{2} \left(1 - \sqrt{\frac{\rho}{2+\rho}} \right) \right]^{2M} \sum_{k=0}^{2M-1} \binom{2M-1+k}{k} \left[\frac{1}{2} \left(1 + \sqrt{\frac{\rho}{2+\rho}} \right) \right]^k. \tag{2.30}$$

At high SNR, (2.30) reduces to [2]

$$P_b \approx \binom{4M-1}{2M} \left(\frac{1}{2\rho} \right)^{2M}, \tag{2.31}$$

and hence a diversity order of $2M$ is achieved.

Alamouti scheme is the basic space-time block code that uses two transmit antennas. With two transmit antennas and M receive antennas, it can achieve full-rate with full-diversity of $2M$ for both real and complex signals. First introduced in 1999

[4], the general space-time block codes based on the theory of orthogonal designs prove to achieve full spatial diversity of $N \times M$. In [4], it was shown that the number of full-rate full-diversity STBC is limited. For complex symbols, the Alamouti scheme is the only full-rate full-diversity STBC. For real symbols, we can find full-rate full-diversity STBC only for 2, 4, and 8 transmit antennas [2][4].

The MIMO-OFCDM systems studied in this thesis are based on two transmit antennas, where Alamouti scheme is employed to achieve transmit diversity.

2.8 Combining Methods

When the transmitted data reaches the receiver side through multiple paths or multiple receive antennas, a suitable combining method is needed to extract data. One group of combining methods is called gain combining, where the received signals from all diversity branches are combined to form the sufficient statistics for data detection. Since the channel gain from all paths are used, this method is called gain combining. A second group of combining methods is selection combining, where the combiner picks the path with the highest SNR and then uses the received signal from this path for detection. Another group of combining methods is hybrid selection/gain combining, where the receiver selects a given number of paths with the highest SNR. Then gain combining methods are used to combine the received signals from these selected branches for detection [5].

2.8.1 Gain Combining

Gain combining methods take the received signals from all branches into account. Simple but efficient gain combining methods are introduced and widely used, which include MRC, EGC, and MMSE combining. In these gain combining methods, the signal used for detection is a linear combination of the received signal from all branches. Hence, the complexity grows linearly with the number of paths. To implement these combining methods, a perfect knowledge of CSI is needed. In a communication system with L paths, let y_l be the received signal from the l-th ($l = 1, 2, ..., L$) path and w_l be the combining weight of the l-th path, then the signal used for detection is given by [5]

$$z = \mathbf{W} \cdot \mathbf{Y} = \sum_{l=1}^{L} w_l \cdot y_l, \tag{2.32}$$

where $\mathbf{W} = \begin{bmatrix} w_1 & w_2 & ... & w_L \end{bmatrix}$, $\mathbf{Y} = \begin{bmatrix} y_1 & y_2 & ... & y_L \end{bmatrix}^{\mathbf{T}}$, and y_l is given by

$$y_l = \sqrt{\frac{E_s}{L}} h_l d_0 + n_l, \tag{2.33}$$

with h_l being the channel coefficient of the l-th path and n_l being the AWGN of the l-th branch with a two-sided power spectral density N_0.

2.8.1.1 MRC

In MRC, the output SNR is maximized by choosing the combining weight w_l as h_l^* [14]. MRC is optimal when the noise on different paths is uncorrelated Gaussian noise. In communication systems involving CDMA, MRC is optimal when no inter-code interference is present [5]. After combining, the signal used for detection is given

by

$$\begin{aligned} z &= \sum_{l=1}^{L} w_l \cdot (\sqrt{\frac{E_s}{L}} h_l d_0 + n_l) \\ &= \sum_{l=1}^{L} \sqrt{\frac{E_s}{L}} |h_l|^2 d_0 + w_l \cdot n_l. \end{aligned} \tag{2.34}$$

Let ρ be the ratio of signal power (averaged over diversity branches) to the noise power,

$$\rho = \frac{E_s}{L \cdot N_0}. \tag{2.35}$$

The instantaneous SNR of the l-th diversity branch, ρ_l, is defined as the ratio the instantaneous signal power at the l-th branch to the noise power of that branch [49]. When MRC is used, ρ_l is given by

$$\rho_l = \rho \cdot \frac{|h_l|^4}{|h_l|^2} = \rho \cdot |h_l|^2 . \tag{2.36}$$

We can define the output SNR as the ratio of the output signal power to the output noise power at the combiner [50]. Then the average output SNR for MRC can be obtained by

$$\rho_{out} = E\left\{\sum_{l=1}^{L} \rho_l\right\} = E\left\{\rho \cdot \sum_{l=1}^{L} |h_l|^2\right\}, \tag{2.37}$$

where $E(\cdot)$ represents expectation operation. When paths are mutually independent and are Rayleigh distributed,

$$\rho_{out} = \rho \cdot L, \tag{2.38}$$

and the symbol error rate is given by [14]

$$P_e = \left[\frac{1 - \sqrt{\rho/(1+\rho)}}{2}\right]^L \sum_{k=0}^{L-1} \binom{L-1+k}{k} \left[\frac{1 + \sqrt{\rho/(1+\rho)}}{2}\right]^k . \tag{2.39}$$

where ρ is defined in (2.35). At high SNR, the symbol error rate can be approximated as [14]

$$P_e \approx (4\rho)^{-L} \binom{2L-1}{L}. \tag{2.40}$$

2.8.1.2 EGC

In EGC, the combining weight is chosen to compensate for the phase of the channel coefficient [51]:

$$w_l = \frac{h_l^*}{|h_l|}. \tag{2.41}$$

That is the received signals from different paths are co-phased and linearly combined to give

$$\begin{aligned} z &= \sum_{l=1}^{L} w_l \cdot (\sqrt{\frac{E_s}{L}} h_l d_0 + n_l) \\ &= \sum_{l=1}^{L} \sqrt{\frac{E_s}{L}} |h_l| \, d_0 + w_l \cdot n_l. \end{aligned} \tag{2.42}$$

In this case, the average output SNR is given by

$$\begin{aligned} \rho_{out} &= E\left\{ \frac{\left| \sum_{l=1}^{L} \sqrt{\frac{E_s}{L}} |h_l| \right|^2}{\sum_{l=1}^{L} |w_l \cdot n_l|^2} \right\} = \frac{\rho}{L} \cdot E\left\{ \left(\sum_{l=1}^{L} |h_l| \right)^2 \right\} \\ &= \frac{\rho}{L} \cdot E\left\{ \sum_{l=1}^{L} |h_l|^2 + \sum_{i=1}^{L} \sum_{\substack{j=1 \\ i \neq j}}^{L} |h_i| \cdot |h_j| \right\}. \end{aligned} \tag{2.43}$$

From the property of complex Gaussian RV we know that for any complex Gaussian RV s with zero mean and variance σ^2, the expected value of $|s|$ is given by [5]

$$E\{|s|\} = \sigma \sqrt{\frac{\pi}{2}}. \tag{2.44}$$

Therefore, when paths are mutually independent and are Rayleigh distributed, the average output SNR can be simplified to [5]

$$\begin{aligned}
\rho_{out} &= \frac{\rho}{L} \cdot E\left\{ \sum_{l=1}^{L} |h_l|^2 + \sum_{i=1}^{L} \sum_{\substack{j=1 \\ i \neq j}}^{L} |h_i| \cdot |h_j| \right\} \\
&= \frac{\rho}{L} \cdot E\left\{ \sum_{l=1}^{L} |h_l|^2 \right\} + E\left\{ \sum_{i=1}^{L} \sum_{\substack{j=1 \\ i \neq j}}^{L} |h_i| \cdot |h_j| \right\} \\
&= \frac{\rho}{L} \cdot \left(L + \frac{L(L-1)}{2} \cdot \sqrt{\frac{\pi}{2}} \cdot \sqrt{\frac{\pi}{2}} \right) \\
&= \rho \cdot \left(1 + (L-1)\frac{\pi}{4} \right). \qquad (2.45)
\end{aligned}$$

Although MRC outperforms EGC in systems without MCI, EGC can achieve full diversity with lower implementation complexity.

2.8.1.3 MMSE Combining

In a multipath fading channel, when the noise on different propagation paths are correlated or when the system has non-Gaussian interference, MMSE combining method becomes the optimal gain combining method [5]. MMSE combining minimizes the mean square error between the transmitted symbol, d_0, and the combiner output, z, [14]:

$$w^* = \arg\min_{w} E\left\{ |z - d_0|^2 \right\}. \qquad (2.46)$$

Hence, the combining weight on the l-th branch is given by [9][10]

$$w_l = \frac{h_l^*}{(1 + K_c)|h_l|^2 + \left(\frac{E_s}{L \cdot N_0}\right)^{-1}}, \qquad (2.47)$$

where K_c is the number of effective interference code channels. It is noted that MMSE combining takes care of the channel phase, the channel gain, the noise power, and the

degree of interference. Therefore, when MCI is high, MMSE combining outperforms both MRC and EGC.

2.8.2 Selection Combining

In selection combining (SC), the combiner selects the signal transmitted on the best reliable channel. The selection criteria can be the highest SNR, the highest absolute power, the lowest error rate, or other criteria, or the combination of these. In a communication system with L independent paths, if the selection is always done based on highest SNR criteria, it can be shown that the diversity gain is equal to L [5]. However, selection combining methods incur some loss in SNR compared to gain combining methods (i.e. not all received signal power is taken into account for decision making in selection combining). Let s_l represent the absolute value of the channel coefficient h_l:

$$s_l = |h_l|\,, \quad l = 1, 2, ..., L. \tag{2.48}$$

Suppose $h_{\max}$ is the channel coefficient with the largest channel gain within these L independent paths, then the possibility that all channel coefficients are less than S is given by

$$\begin{aligned} P\left(|h_{\max}| \leq S\right) &= P\left(s_{\max} \leq S\right) \\ &= P\left(s_1, s_2, ..., s_L \leq S\right). \end{aligned} \tag{2.49}$$

Taking the derivative of (2.49), we can obtain $p_{s_{\max}}(s)$, the PDF of s. Since the combiner in SC selects only the received signal from the best path, the instantaneous received signal power is $\frac{P_s}{L}\left|h_{\max}\right|^2$, where $\frac{P_s}{L}$ is the average transmitted power allocated

to each diversity branch for each symbol. Therefore, the average signal power used for decision making at the SC combiner output can be calculated by

$$P_{selection} = \int_0^{+\infty} \frac{P_s}{L} \cdot s^2 \cdot p_{s_{\max}}(s) ds. \tag{2.50}$$

We can see that for each symbol, $P_{selection}$ is only a portion of $P_s \times L$, the total transmitted signal power, and the ratio between them is

$$\frac{P_{selection}}{P_s} = \int_0^{+\infty} s^2 \cdot p_{s_{\max}}(s) ds. \tag{2.51}$$

Nevertheless, the advantage of selection combining is that it achieves the same diversity gain as a full system but with less hardware (i.e. RF chains).

2.8.3 Hybrid Selection/Gain Combining

In hybrid selection/gain combining, the combiner selects the best L_s paths out of L paths and then uses a gain combining method to combine the signals for detection [5][49]. Same as SC, hybrid selection/gain combining can extract diversity gain of L and uses less hardware to implement. However, hybrid selection/gain combining allows to choose the number of paths. As the number of selected paths increases, the received SNR gain increases, but the complexity of detection grows as well. This flexibility makes hybrid selection/gain combining adaptable in different applications.

2.9 Conclusion

In this chapter, key concepts related to this thesis were reviewed. First, commonly used channel models were presented. Then different technologies such as OFDM, CDMA, which are used in wireless communications to support multi-user environment

were discussed. Finally we studied how to achieve transmit and receive diversity with STBC and different combining schemes. Having understood those concepts, we will be able to present the study in this thesis.

CHAPTER 3

SISO-OFCDM SYSTEMS

In this chapter, we will study the performance of SISO-OFCDM systems. First we will introduce the system model of SISO-OFCDM. Then we will look into the detection algorithm and present system performance evaluations for MRC, EGC, and MMSE combining methods. Finally we provide simulation results for different SISO-OFCDM systems.

3.1 System Model

The transmitter structure of an OFCDM system is shown in Figure 3.1. The user data is firstly processed by a modulator such as BPSK. When using QPSK or higher order modulation, Grey coding should be employed. The modulated symbols are then converted from a serial symbol stream into N_B parallel symbol streams, where N_B is the number of user data that will be two-dimensionally spread with the same spreading code. The spreading is provided by a spreading code generator, and each group of N_B symbols will be spread with a unique code. In the OFCDM system, let the spreading factor in frequency domain and time domain be N_F and N_T respectively, then the length of spreading code, N_S, is given by

$$N_S = N_T \times N_F. \tag{3.1}$$

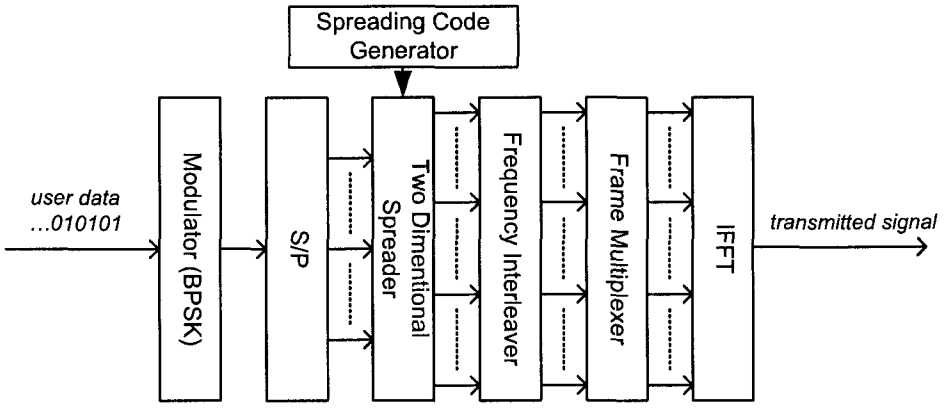

Figure 3.1: Transmitter structure of SISO-OFCDM system

Since the overall spreading factor is N_S, a maximum N_S different codes are available for spreading. Let K be the number of actually transmitted groups, and each group of data symbol is assigned with a unique spreading code, then $K \leq N_S$. And if different data symbols are from different system users, a maximum $K \times N_B$ users can access the system at the same time. The system load, denoted by ζ, is defined as the number of spreading codes assigned divided by the total number of spreading codes available, which is given by

$$\zeta = \frac{K}{N_S}. \tag{3.2}$$

When the system is running at full load, $N_S \times N_B$ symbols can be transmitted at the same time.

The overall spreading code C is a combination of frequency domain spreading code C^F and time domain spreading code C^T. Here, both C^F and C^T are OVSF codes. Let $C(k)$ represent the k-th $(k = 0, 1, ..., K-1)$ spreading code, $C^F(i)$ represent the i-th $(i = 0, 1, ..., N_F - 1)$ frequency domain OVSF spreading code of length N_F,

$C^T(j)$ represent the j-th ($j = 0, 1, ..., N_T - 1$) time domain OVSF spreading code of length N_T, denoted respectively as

$$C(k) = \begin{bmatrix} c_0(k) & c_1(k) & ... & c_{N_F-1}(k) \\ c_{N_F}(k) & c_{N_F+1}(k) & ... & c_{2N_F-1}(k) \\ ... & ... & ... & ... \\ c_{N_TN_F}(k) & c_{N_TN_F+1}(k) & ... & c_{N_S-1}(k) \end{bmatrix}, \quad k = 0, 1, ..., K-1 \tag{3.3}$$

$$C^F(i) = \begin{bmatrix} c_0^F(i) & c_1^F(i) & ... & c_{N_F-1}^F(i) \end{bmatrix}, \quad i = 0, 1, ..., N_F - 1 \tag{3.4}$$

$$C^T(j) = \begin{bmatrix} c_0^T(j) & c_1^T(j) & ... & c_{N_T-1}^T(j) \end{bmatrix}, \quad j = 0, 1, ..., N_T - 1. \tag{3.5}$$

Our study focuses on downlink transmission in OFCDM systems, where we assume perfect synchronization. Also, we assume each sub-carrier experiences flat fading in our study, so the orthogonality of the OVSF code in time domain is preserved. However, the orthogonality in frequency domain is distorted because of different fading among different sub-carriers. With an example, it is easier to understand why the orthogonality is lost. Assuming a simple OFCDM system with $N_F = 2$ and $N_T = 1$, then $C^F(0) = \begin{bmatrix} 1 & 1 \end{bmatrix}$, $C^F(1) = \begin{bmatrix} 1 & -1 \end{bmatrix}$, and $C^T(0) = [1]$. When two data symbols, denoted as α_1 and α_2, are spread with $C^F(0)$ and $C^F(1)$ respectively and then transmitted, the received signal is given by

$$\begin{aligned} \beta_1 &= \sqrt{E_s} \cdot h_1 \cdot \left[\alpha_1 c_0^F(0) + \alpha_2 c_1^F(0)\right] \cdot c_0^T(0) + n_1 \\ &= \sqrt{E_s} \cdot h_1 \cdot [\alpha_1 + \alpha_2] + n_1 \end{aligned} \tag{3.6}$$

$$\begin{aligned} \beta_2 &= \sqrt{E_s} \cdot h_2 \cdot \left[\alpha_1 c_0^F(1) + \alpha_2 c_1^F(1)\right] \cdot c_0^T(0) + n_2 \\ &= \sqrt{E_s} \cdot h_2 \cdot [\alpha_1 - \alpha_2] + n_2, \end{aligned} \tag{3.7}$$

where h_1 and h_2 are the two corresponding fading coefficients, and n_1 and n_2 are additive noise terms at the receiver side. If we use decoding technique for CDMA to detect α_1 and α_2, the decision variables will be

$$\begin{aligned}\widehat{\alpha}_1 &= \frac{1}{2}\left[\beta_1 c_0^F(0) + \beta_2 c_0^F(1)\right] \\ &= \sqrt{E_s}\cdot\left(\frac{h_1+h_2}{2}\right)\cdot\alpha_1 + \sqrt{E_s}\cdot\left(\frac{h_1-h_2}{2}\right)\cdot\alpha_2 + \frac{n_1+n_2}{2} \qquad (3.8)\end{aligned}$$

$$\begin{aligned}\widehat{\alpha}_2 &= \frac{1}{2}\left[\beta_1 c_1^F(0) + \beta_2 c_1^F(1)\right] \\ &= \sqrt{E_s}\cdot\left(\frac{h_1+h_2}{2}\right)\cdot\alpha_2 + \sqrt{E_s}\cdot\left(\frac{h_1-h_2}{2}\right)\cdot\alpha_1 + \frac{n_1+n_2}{2}. \qquad (3.9)\end{aligned}$$

The terms $\sqrt{E_s}\cdot\left(\frac{h_1-h_2}{2}\right)\cdot\alpha_2$ in (3.8) and $\sqrt{E_s}\cdot\left(\frac{h_1-h_2}{2}\right)\cdot\alpha_1$ in (3.9) represent MCI, which is introduced as long as the channels h_1 and h_2 are not identical.

From the example above we can see that MCI is generated when different users' data is spread with different frequency domain spreading codes and the same time domain spreading code. To overcome this, the spreading code should be designed in such way to take advantage of the orthogonality in time domain. Specifically, the spreading code generator minimizes the number of frequency domain OVSF spreading codes used. Therefore, the level of MCI is minimized. Here we use an example to illustrate how to generate the spreading codes. When $N_F = 2$ and $N_T = 4$, $C(0)$ is generated by $C^F(0) = \begin{bmatrix} 1 & 1 \end{bmatrix}$ and $C^T(0) = \begin{bmatrix} 1 & 1 & 1 & 1 \end{bmatrix}$:

$$\begin{aligned}C(0) &= \left[C^F(0)\right]^{\mathbf{T}}\cdot C^T(0) \\ &= \begin{bmatrix} 1 & 1 & 1 & 1 \\ 1 & 1 & 1 & 1 \end{bmatrix},\end{aligned}$$

$C(1)$ is generated by $C^F(0)$ and $C^T(1) = \begin{bmatrix} 1 & 1 & -1 & -1 \end{bmatrix}$:

$$\begin{aligned} C(1) &= \left[C^F(0)\right]^{\mathbf{T}} \cdot C^T(1) \\ &= \begin{bmatrix} 1 & 1 & -1 & -1 \\ 1 & 1 & -1 & -1 \end{bmatrix}, \end{aligned}$$

$C(2)$ is generated by $C^F(0)$ and $C^T(2) = \begin{bmatrix} 1 & -1 & 1 & -1 \end{bmatrix}$:

$$\begin{aligned} C(2) &= \left[C^F(0)\right]^{\mathbf{T}} \cdot C^T(2) \\ &= \begin{bmatrix} 1 & -1 & 1 & -1 \\ 1 & -1 & 1 & -1 \end{bmatrix}, \end{aligned}$$

and so forth. Until the time domain OVSF spreading code is used up, the code generator will change the frequency domain OVSF spreading code and restarts the cycle. Therefore, $C(N_T)$ is generated by $C^F(1)$ and $C^T(0)$, $C(N_T+1)$ is generated by $C^F(1)$ and $C^T(1)$, $C(N_T+2)$ is generated by $C^F(1)$ and $C^T(2)$, and so forth. In the example when $N_F = 2$ and $N_T = 4$, $C(N_T) = C(4)$ is given by

$$\begin{aligned} C(4) &= \left[C^F(1)\right]^{\mathbf{T}} \cdot C^T(0) \\ &= \begin{bmatrix} 1 & -1 \end{bmatrix}^{\mathbf{T}} \cdot \begin{bmatrix} 1 & 1 & 1 & 1 \end{bmatrix} \\ &= \begin{bmatrix} 1 & 1 & 1 & 1 \\ -1 & -1 & -1 & -1 \end{bmatrix}, \end{aligned}$$

$C(N_T+1) = C(5)$ is given by

$$\begin{aligned} C(5) &= \left[C^F(1)\right]^{\mathbf{T}} \cdot C^T(1) \\ &= \begin{bmatrix} 1 & 1 & -1 & -1 \\ -1 & -1 & 1 & 1 \end{bmatrix}. \end{aligned}$$

By assigning spreading codes according to this method, one can see that MCI will be present if $K > N_T$. When $K \leq N_T$, data symbols transmitted by the same N_F carriers are spread with the same frequency domain spreading code but different time domain spreading codes. In this case, no MCI is present in the system. However, when $K > N_T$, at least two data symbols are spread with different frequency domain spreading codes but the same time domain spreading code, and MCI occurs. For any given spreading code $C(k)$ $(k = 0, 1, ..., K-1)$, let K_c be the number of interfering codes. When the spreading codes are generated according to the method explained above, K_c is given by the number of codes that have the same time domain spreading code as $C(k)$ but different frequency domain spreading codes.

Take the system with $N_F = 2$ and $N_T = 4$ for example. When $K \leq 4$, the spreading codes $C(0)$, $C(1)$, ..., $C(K-1)$ are generated from $C^F(0)$ with different time domain spreading codes, so no MCI is present and $K_c = 0$. On the other hand, consider the case when $K = 6$. $C(0)$ and $C(4)$ are generated from the same time domain spreading code $C^T(0)$ with different frequency domain spreading codes $C^F(0)$ and $C^F(1)$ respectively. Thus, $C(0)$ and $C(4)$ interfere with each other. Also, since $C(1)$ and $C(5)$ are generated from $C^T(1)$ with $C^F(0)$ and $C^F(1)$ respectively, they interfere with each other. Therefore, $K_c = 1$ for $C(0)$, $C(1)$, $C(4)$ and $C(5)$, but $K_c = 0$ for $C(2)$ and $C(3)$. One can generalize the relationship between K_c and K as

$$\left\lfloor \frac{K-1}{N_T} \right\rfloor - 1 \leq K_c \leq \left\lfloor \frac{K-1}{N_T} \right\rfloor, \text{ when } K > N_T. \tag{3.10}$$

where the operator $\lfloor x \rfloor$ represents the integer portion of x with $\lfloor x \rfloor \leq x$.

From this spreading codes generating method, one can see that when the code

$C(k)$ $(k = 0, 1, ..., K-1)$ is generated by $C^F(i)$ and $C^T(j)$, the relationship between k, i, and j is

$$i = \left\lfloor \frac{k}{N_T} \right\rfloor, \tag{3.11}$$

$$\begin{aligned} j &= k \bmod N_T \\ &= k - N_T \cdot \left\lfloor \frac{k}{N_T} \right\rfloor. \end{aligned} \tag{3.12}$$

The spreading factor in frequency domain is N_F, where N_F sub-carriers are dedicated to transmit the same data symbol. In order to minimize the correlation among those N_F sub-carriers, one should ensure that sub-carriers are separated enough using interleaving. The interleaving should be carried out as follows. In a group of N_B symbols that is spread with the same spreading code, the first symbol is spread into the zeroth, N_B-th, $(2N_B)$-th, ..., and $[(N_F - 1) \cdot N_B]$-th sub-carriers, the second symbol is spread into the first, $(N_B + 1)$-th, $(2N_B + 1)$-th, ..., and $[(N_F - 1) \cdot N_B + 1]$-th sub-carriers, and so forth. Finally, the N_B-th symbol is spread into the $(N_B - 1)$-th, $(2N_B - 1)$-th, ..., and $(L - 1)$-th sub-carriers, where $L = N_F \cdot N_B$ is the total number of sub-carriers employed in the OFCDM system.

Let us take for example the j-th $(j = 1, 2, ..., N_B)$ symbol in the k-th $(k = 0, 1, ..., K-1)$ group. The two-dimensional spreading and frequency interleaving is presented in Figure 3.2. The spreading code assigned to this symbol is $C(k)$ and the time domain spreading factor is N_T. Then the first N_T chips of $C(k)$, $\{c_0(k), c_1(k), c_2(k), ..., c_{N_T-1}(k)\}$, are transmitted on the $(j-1)$-th sub-carrier; the second N_T chips of $C(k)$, $\{c_{N_T}(k), c_{N_T+1}(k), c_{N_T+2}(k), ..., c_{2N_T-1}(k)\}$, on the $(j - 1 + N_B)$-th sub-carrier; $\{c_{2N_T}(k), c_{2N_T+1}(k), c_{2N_T+2}(k), ..., c_{3N_T-1}(k)\}$ on the $(j - 1 + 2N_B)$-th

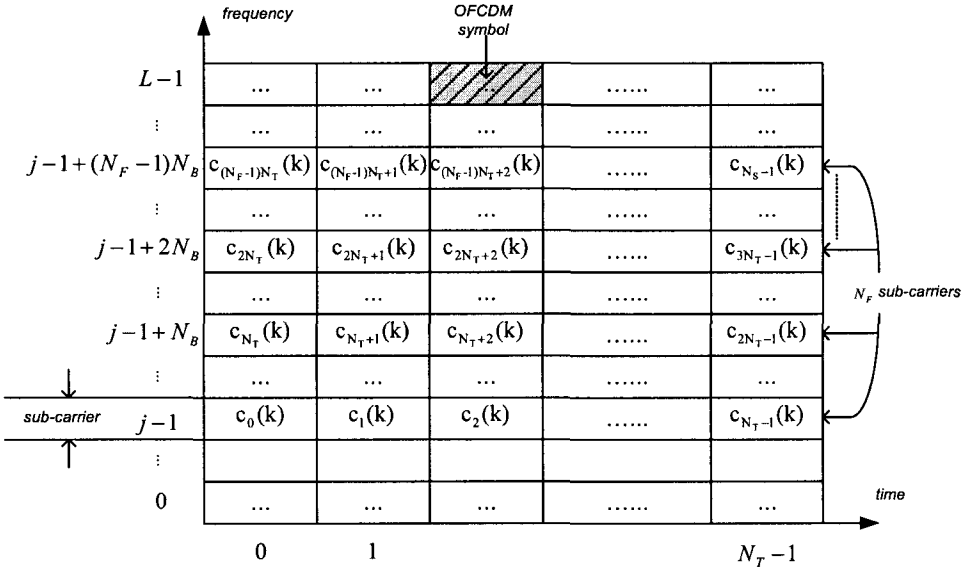

Figure 3.2: Two-dimensional spreading and frequency interleaving

sub-carrier; and so forth. Finally, the last N_T chips of $C(k)$ are transmitted on the $(j-1+(N_F-1)N_B)$-th sub-carrier.

As shown in Figure 3.2, a signal transmitted during one time slot on one sub-carrier in OFCDM system is called an OFCDM symbol. After two-dimensional spreading and frequency interleaving for a group of N_B modulated symbols, an OFCDM frame consisting of $L \times N_T$ OFCDM symbols is constructed. Assigned with different spreading codes, in total K OFCDM frames are multiplexed to build a super-frame, and this step is done by a frame multiplexer, shown in Figure 3.3.

Let the indices l_0,l_1,...,l_{N_F-1} represent the N_F sub-carriers carrying the k-th user data after frequency interleaving. In an OFCDM super-frame, the OFCDM symbol on the l_i-th $(i = 0, 1, ..., N_F - 1)$ sub-carrier during the j-th $(j = 0, 1, ..., N_T - 1)$ time

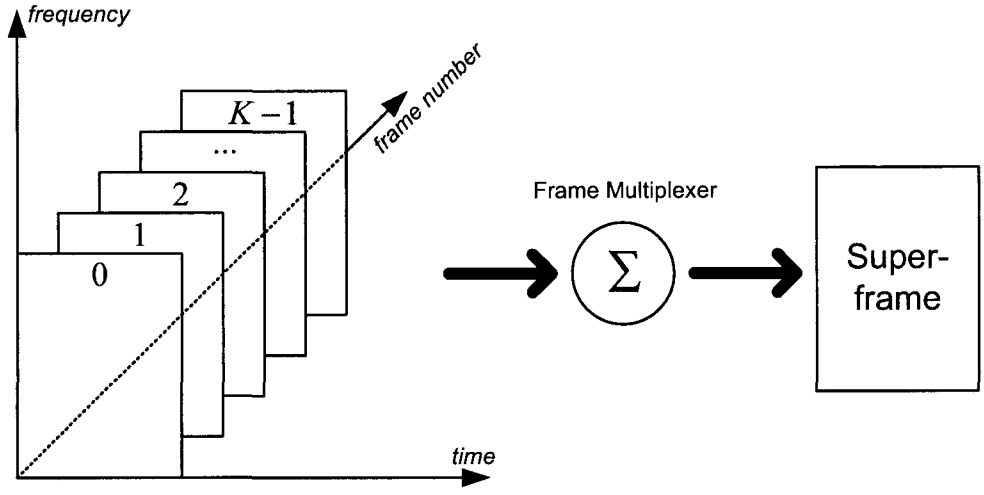

Figure 3.3: Multiplexing K frames into a superframe

slot can be expressed as

$$s(l_i, j) = \sqrt{\frac{E_s}{N_S}} \sum_{k=0}^{K-1} d_k c_{\lfloor \frac{l_i}{N_B} \rfloor N_T + j}(k), \tag{3.13}$$

where d_k is the k-th user data on the l_i-th sub-carrier, $c_{\lfloor \frac{l_i}{N_B} \rfloor N_T + j}(k)$ is the $(\left\lfloor \frac{l_i}{N_B} \right\rfloor N_T + j)$-th chip of the k-th user's spreading code, $\left\lfloor \frac{l_i}{N_B} \right\rfloor$ is the chip index of the frequency domain spreading code, j is the chip index of the time domain spreading code, and E_s is the total transmitted signal energy for each symbol. Since each data symbol is spread on N_S OFCDM symbols, the total transmitted power has to be averaged over these N_S OFCDM symbols. After frame multiplexing, the OFCDM super-frame is transmitted through a SISO-OFDM transmission system. The transmitted OFCDM symbols on different sub-carriers experience different fades. In this work, within one OFCDM super-frame, the OFCDM symbols transmitted on the same sub-carrier experience the same fading (i.e. fading is fixed for one OFCDM frame duration).

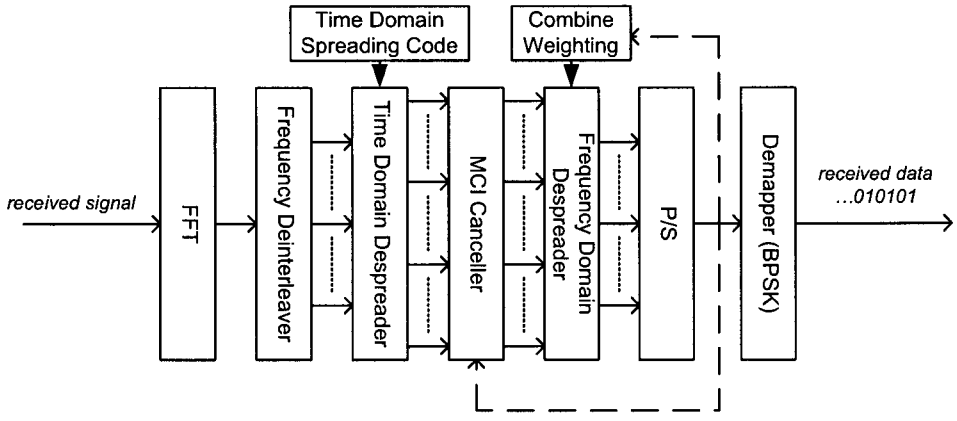

Figure 3.4: Receiver structure of SISO-OFCDM system

The receiver structure is shown in Figure 3.4. Let $\mathbf{r}(l_i, j)$ denote the received OFCDM symbol on the l_i-th sub-carrier during the j-th time slot:

$$\begin{aligned}\mathbf{r}(l_i, j) &= \sum_{k=0}^{K-1} \left(\sqrt{\frac{E_s}{N_S}} \cdot h_{l_i} \cdot d_k \cdot c_{\lfloor \frac{l_i}{N_B} \rfloor N_T + j}(k) \right) + \eta(l_i, j) \\ &= \sqrt{\frac{E_s}{N_S}} \cdot h_{l_i} \cdot \sum_{k=0}^{K-1} d_k \cdot c_{\lfloor \frac{l_i}{N_B} \rfloor N_T + j}(k) + \eta(l_i, j), \end{aligned} \tag{3.14}$$

where $\eta(l_i, j)$ is the AWGN on the l_i-th sub-carrier during the j-th time slot.

3.2 Detection Algorithm

At the receiver side, the received signal is first frequency deinterleaved to form N_B groups. Each group has N_F received signals from the N_F sub-carriers carrying the same user data. In each group, there are K users' data multiplexed by different spreading codes. Then, time domain despreading is carried out. After despreading the N_F signals in time domain, to sort out each of the K users' data, the output of

the k-th user despreader is

$$\begin{aligned} r_k(l_i) &= \frac{1}{N_T}\sum_{j=0}^{N_T-1}\mathbf{r}(l_i,j).c_j^T(k) \\ &= \sqrt{\frac{E_s}{N_S}}\cdot h_{l_i}\cdot d_k c^F_{\left\lfloor\frac{l_i}{N_B}\right\rfloor}(k)+\overline{\eta}(l_i), \end{aligned} \tag{3.15}$$

where $c_j^T(k)$ is the j-th chip of the k-th time domain OVSF code, and $\overline{\eta}(l_i)$ is the equivalent noise added to the l_i-th sub-carrier.

Let σ_n^2 represent the noise energy added to each OFCDM symbol:

$$E\left\{|\eta(l_i,j)|^2\right\}=\sigma_n^2, \tag{3.16}$$

then the variance of $\overline{\eta}(l_i)$ at each dimension is given by

$$\begin{aligned} E\left\{|\overline{\eta}(l_i)|^2\right\} &= E\left\{\frac{1}{N_T}\sum_{i=0}^{N_T-1}|\eta(l_i,j)|^2\right\} \\ &= \frac{1}{N_T^2}E\left\{\sum_{i=0}^{N_T-1}|\eta(l_i,j)|^2\right\} \\ &= \frac{1}{N_T}E\left\{|\eta(l_i,j)|^2\right\} \\ &= \frac{\sigma_n^2}{N_T}. \end{aligned} \tag{3.17}$$

From the design of the spreading code described above, one can see that the system will introduce MCI if the number of multiplexed frames K is greater than the number of available time domain spreading codes N_T. In the case when MCI is present, an interference canceller is used to cancel the MCI in an iterative way after time domain despreading [9]. In this thesis, we focus on OFCDM systems with no MCI. In what follows, we analyze the performance of this system in terms of its BER.

After time domain despreading, a suitable combining method is employed to combine the N_F signals, $r_k(l_i)$ $(i = 0, 1, ..., N_F - 1)$, for the k-th user. In what

follows, we study MRC, EGC, and MMSE combining methods. In these methods, the combining weight $w(l_i)$ $(i = 0, 1, ..., N_F - 1)$ of each sub-carrier calculated and used in frequency domain despreading is given by

- for MRC [14],

$$w(l_i) = h_{l_i}^*, \tag{3.18}$$

- for EGC [51],

$$w(l_i) = \frac{h_{l_i}^*}{|h_{l_i}|}, \tag{3.19}$$

- for MMSE combining [9][10],

$$\begin{aligned} w(l_i) &= \frac{h_l^*}{(1+K_c)|h_{l_i}|^2 + \left(\frac{E_s}{N_F \cdot N_0}\right)^{-1}} \\ &= \frac{h_l^*}{(1+K_c)|h_{l_i}|^2 + \left(\frac{\widetilde{\rho}}{N_F}\right)^{-1}}, \end{aligned} \tag{3.20}$$

where E_s is the total transmitted energy for each data symbol over all the N_F sub-carriers, N_0 is the power spectral density of the AWGN added to each OFCDM symbol, $\widetilde{\rho}$ is defined as the ratio of total transmitted power of each data symbol to the background noise power, and K_c is the number of interfering codes. For any transmitted data symbol, K_c is given by the number of data symbols that are spread with the same time domain spreading code but different frequency domain spreading codes. In an OFCDM system with no MCI, the combining weight of the MMSE combining becomes

$$w(l_i) = \frac{h_{l_i}^*}{|h_{l_i}|^2 + \left(\frac{\widetilde{\rho}}{N_F}\right)^{-1}}. \tag{3.21}$$

In general, the output of the frequency domain despreader is given by

$$y_k = \sum_{i=0}^{N_F-1} r_k(l_i) \cdot c^F_{\left\lfloor \frac{l_i}{N_B} \right\rfloor}(k) \cdot w(l_i). \tag{3.22}$$

This output is then normalized to form the decision variable, z_k, which will be used in MCI cancellation for systems with MCI:

$$z_k = \frac{1}{\sqrt{\frac{E_s}{N_S}}} \cdot \frac{y_k}{\sum_{i=0}^{N_F-1} h_{l_i} \cdot w(l_i)}. \tag{3.23}$$

Finally a hard decision based on minimum distance criteria is made to recover the corresponding user data:

$$\widehat{d_k} = \arg\min_{\{s\}} |z_k - s|^2, \tag{3.24}$$

where $\{s\}$ is the set of all possible transmitted data symbols.

3.3 Performance Evaluation

In this section, we present semi-analytical results for the BER of OFCDM systems over flat fading channels with MRC, EGC, and MMSE combining. We assume binary phase-shift keying (BPSK) is used to modulate user data.

In what follows, we use the notation $\overrightarrow{e}$ to represent the error vector between the

decision variable z_k and the transmitted BPSK symbol d_k, where $\overrightarrow{e}$ is given by

$$\begin{aligned}
\overrightarrow{e} &= z_k - d_k \\
&= \frac{\sum_{i=0}^{N_F-1} r_k(l_i) c^F_{\left\lfloor \frac{l}{N_B} \right\rfloor}(k) w(l_i)}{\sqrt{\frac{E_s}{N_S}} \sum_{i=0}^{N_F-1} h(l_i) w(l_i)} - d_k \\
&= \frac{\sum_{i=0}^{N_F-1} \left[\left(\sqrt{\frac{E_s}{N_S}} h_{l_i} d_k c^F_{\left\lfloor \frac{l}{N_B} \right\rfloor}(k) + \overline{\eta}(l_i) \right) c^F_{\left\lfloor \frac{l}{N_B} \right\rfloor}(k) - \sqrt{\frac{E_s}{N_S}} h_{l_i} d_k \right] w(l_i)}{\sqrt{\frac{E_s}{N_S}} \sum_{i=0}^{N_F-1} h_{l_i} w(l_i)} \\
&= \frac{\sum_{i=0}^{N_F-1} \overline{\overline{\eta}}(l_i) \cdot w(l_i)}{\sqrt{\frac{E_s}{N_S}} \cdot \sum_{i=0}^{N_F-1} h_{l_i} \cdot w(l_i)},
\end{aligned} \tag{3.25}$$

with $\overline{\overline{\eta}}(l_i)$ being the equivalent complex Gaussian noise on the l_i-th sub-carrier, with zero mean and variance $\sigma^2_{\overline{\overline{\eta}}} = \frac{\sigma^2_\eta}{N_T}$. Let $\widetilde{\rho}$ be the ratio of total transmitted signal power for each symbol to the background noise power. Since the additive noise term $\eta(l,i)$ is complex AWGN with variance 0.5 per dimension, then $\widetilde{\rho} = E_S$, and the error vector, $\overrightarrow{e}$, becomes

$$\overrightarrow{e} = \frac{\sum_{i=0}^{N_F-1} \overline{\overline{\eta}}(l_i) \cdot w(l_i)}{\sqrt{\frac{\widetilde{\rho}}{N_S}} \cdot \sum_{i=0}^{N_F-1} h_{l_i} \cdot w(l_i)}, \tag{3.26}$$

with $\sigma^2_{\overline{\overline{\eta}}} = \frac{1}{N_T}$. Conditioned on the channel, $\sum_{i=0}^{N_F-1} \overline{\overline{\eta}}(l_i) \cdot w(l_i)$ is Gaussian with zero mean and variance

$$\sigma^2_{\overline{\overline{\eta}}} = \frac{1}{N_T} \sum_{i=0}^{N_F-1} |w(l_i)|^2 . \tag{3.27}$$

In the case when MCI is present, if K_c is greater than 50 [12], the MCI can be considered as an additive Gaussian noise added to each OFCDM symbol with zero

mean and variance σ_I^2 given by [11][12]

$$\sigma_I^2 = \frac{2K_c E_s}{N_F N_S} \left| \sum_{i=0}^{N_F-1} \left[h_{l_i} \cdot w(l_i) \right]^2 - \left\{ \sum_{i=0}^{N_F-1} \left[h_{l_i} \cdot w(l_i) \right] \right\}^2 \right|. \tag{3.28}$$

Since σ_η^2 and σ_I^2 are independent, the total system noise can be approximated as $\left(\sigma_\eta^2 + \sigma_I^2\right)$ when evaluating the probability of bit error.

In what follows, we evaluate the performance of MRC, EGC, and MMSE combining respectively when no MCI is present. MRC maximizes the output SNR [5], so it performs better than EGC and MMSE combining in OFCDM systems without MCI. EGC is simple to implement since only the phases of the channels are compensated. MMSE combining corrects the phase shift and the attenuation of the channel fading at the same time, which makes it the only adaptive method among these three methods. Therefore, in the presence of MCI, MMSE combining becomes optimal and outperforms both MRC and EGC [5].

3.3.1 MRC

With MRC, the combining weight of each sub-carrier is given by [14]:

$$w(l) = h_l^*, \tag{3.29}$$

and the error vector, $\overrightarrow{e}$, becomes

$$\overrightarrow{e} = \frac{\sum_{i=0}^{N_F-1} \overline{\overline{\eta}}(l_i) \cdot w(l_i)}{\sqrt{\frac{\tilde{\rho}}{N_S}} \cdot \sum_{i=0}^{N_F-1} h_{l_i} \cdot w(l_i)} = \frac{\sum_{i=0}^{N_F-1} \overline{\overline{\eta}}(l_i) h_{l_i}^*}{\sqrt{\frac{\tilde{\rho}}{N_S}} \cdot \sum_{i=0}^{N_F-1} |h_{l_i}|^2}, \tag{3.30}$$

with

$$\sigma_{\tilde{\eta}}^2 = \frac{1}{N_T} \sum_{i=0}^{N_F-1} |w(l_i)|^2 = \frac{1}{N_T} \sum_{i=0}^{N_F-1} |h_{l_i}|^2 . \tag{3.31}$$

When BPSK modulation is used, the probability of bit error conditioned on the channel is given by

$$\begin{aligned} P_e|_h &= P\left(\mathrm{Re}(\overrightarrow{e}) > 1\right) \\ &= P\left(\mathrm{Re}\left(\frac{\sum_{i=0}^{N_F-1}\overline{\overline{\eta}}(l_i)h_{l_i}^*}{\sqrt{\frac{\widetilde{\rho}}{N_S}}\cdot\sum_{i=0}^{N_F-1}|h_{l_i}|^2}\right) > 1\right) \\ &= P\left(\mathrm{Re}\left(\sum_{m=0}^{N_F-1}\overline{\overline{\eta}}(l_i)h_{l_i}^*\right) > \sqrt{\frac{\widetilde{\rho}}{N_S}}\cdot\sum_{i=0}^{N_F-1}|h_{l_i}|^2\right) \\ &= Q\left(\frac{\sqrt{\frac{\widetilde{\rho}}{N_S}}\cdot\sum_{i=0}^{N_F-1}|h_{l_i}|^2}{\sqrt{\frac{1}{2N_T}\sum_{i=0}^{N_F-1}|h_{l_i}|^2}}\right) \\ &= Q\left(\sqrt{\frac{2\widetilde{\rho}}{N_F}\sum_{i=0}^{N_F-1}|h_{l_i}|^2}\right), \end{aligned} \tag{3.32}$$

where $Q(\cdot)$ is defined as [14]

$$Q(x) = \int_x^\infty \frac{1}{\sqrt{2\pi}} e^{-\frac{v^2}{2}}\mathrm{d}v. \tag{3.33}$$

3.3.2 EGC

As mentioned before, with EGC, the combining weight of each sub-carrier is chosen to compensate for the phase shift of the fading coefficient [51]:

$$w(l) = \frac{h_l^*}{|h_l|}. \tag{3.34}$$

The error vector becomes

$$\overrightarrow{e} = \frac{\sum_{i=0}^{N_F-1}\overline{\overline{\eta}}(l_i)\cdot w(l_i)}{\sqrt{\frac{\widetilde{\rho}}{N_S}}\cdot\sum_{i=0}^{N_F-1}h_{l_i}\cdot w(l_i)} = \frac{\sum_{i=0}^{N_F-1}\overline{\overline{\eta}}(l_i)\frac{h_l^*}{|h_l|}}{\sqrt{\frac{\widetilde{\rho}}{N_S}}\cdot\sum_{i=0}^{N_F-1}|h_{l_i}|}, \tag{3.35}$$

and

$$\sigma_{\tilde{\eta}}^2 = \frac{1}{N_T}\sum_{i=0}^{N_F-1}|w(l_i)|^2 = \frac{1}{N_T}\sum_{i=0}^{N_F-1}\left|\frac{h_{l_i}^*}{h_{l_i}}\right|^2 = \frac{N_F}{N_T}. \tag{3.36}$$

Similar to the approach in MRC, the probability of bit error conditioned on the channel with EGC is given by

$$\begin{aligned} P_e|_h &= P\left(\mathrm{Re}(\overrightarrow{e}) > 1\right) \\ &= P\left(\mathrm{Re}\left(\frac{\sum_{i=0}^{N_F-1}\overline{\overline{\eta}}(m_i)\frac{h_l^*}{|h_l|}}{\sqrt{\frac{\tilde{\rho}}{N_S}}\cdot\sum_{i=0}^{N_F-1}|h_{l_i}|}\right) > 1\right) \\ &= Q\left(\frac{\sqrt{\frac{\tilde{\rho}}{N_S}}\cdot\sum_{i=0}^{N_F-1}|h_{l_i}|}{\sqrt{\frac{N_F}{2N_T}}}\right) \\ &= Q\left(\frac{\sqrt{2\tilde{\rho}}}{N_F}\sum_{i=0}^{N_F-1}|h_{l_i}|\right). \end{aligned} \tag{3.37}$$

3.3.3 MMSE Combining

For MMSE combining with no MCI, the combining weight is given by[9][10],

$$w(l) = \frac{h_l^*}{|h_l|^2 + \left(\frac{\tilde{\rho}}{N_F}\right)^{-1}}. \tag{3.38}$$

Then the error vector $\overrightarrow{e}$ becomes

$$\overrightarrow{e} = \frac{\sum_{i=0}^{N_F-1}\overline{\overline{\eta}}(l_i)\cdot w(l_i)}{\sqrt{\frac{\tilde{\rho}}{N_S}}\cdot\sum_{i=0}^{N_F-1}h_{l_i}\cdot w(l_i)} = \frac{\sum_{i=0}^{N_F-1}\overline{\overline{\eta}}(l_i)\frac{h_{l_i}^*}{|h_{l_i}|^2+\left(\frac{\tilde{\rho}}{N_F}\right)^{-1}}}{\sqrt{\frac{\tilde{\rho}}{N_S}}\cdot\sum_{i=0}^{N_F-1}\frac{|h_{l_i}|^2}{|h_{l_i}|^2+\left(\frac{\tilde{\rho}}{N_F}\right)^{-1}}}, \tag{3.39}$$

and

$$\sigma_{\tilde{\eta}}^2 = \frac{1}{N_T}\sum_{i=0}^{N_F-1}|w(l_i)|^2 = \frac{1}{N_T}\sum_{i=0}^{N_F-1}\frac{|h_{l_i}|^2}{\left[|h_{l_i}|^2 + \left(\frac{\tilde{\rho}}{N_F}\right)^{-1}\right]^2}. \tag{3.40}$$

The probability of bit error conditioned on the channel is given by

$$
\begin{aligned}
P_e|_h &= P\left(\mathrm{Re}(\overrightarrow{e}) > 1\right) \\
&= P\left(\mathrm{Re}\left(\frac{\sum_{i=0}^{N_F-1} \overline{\overline{\eta}}(l_i) \frac{h_{l_i}^*}{|h_{l_i}|^2 + \left(\frac{\tilde{\rho}}{N_F}\right)^{-1}}}{\sqrt{\frac{\tilde{\rho}}{N_S}} \cdot \sum_{i=0}^{N_F-1} \frac{|h_{l_i}|^2}{|h_{l_i}|^2 + \left(\frac{\tilde{\rho}}{N_F}\right)^{-1}}}\right) > 1\right) \\
&= Q\left(\frac{\sqrt{\frac{\tilde{\rho}}{N_S}} \cdot \sum_{i=0}^{N_F-1} \frac{|h_{l_i}|^2}{|h_{l_i}|^2 + \left(\frac{\tilde{\rho}}{N_F}\right)^{-1}}}{\sqrt{\frac{1}{2N_T} \sum_{i=0}^{N_F-1} \frac{|h_{l_i}|^2}{\left[|h_{l_i}|^2 + \left(\frac{\tilde{\rho}}{N_F}\right)^{-1}\right]^2}}}\right) \\
&= Q\left(\frac{\sqrt{2} \sum_{i=0}^{N_F-1} \frac{1}{1 + \left(\frac{\tilde{\rho}}{N_F}\right)^{-1} \cdot |h_{l_i}|^{-2}}}{\sqrt{\sum_{i=0}^{N_F-1} \frac{1}{\frac{\tilde{\rho}}{N_F} \cdot |h_{l_i}|^2 + 2 + \left(\frac{\tilde{\rho}}{N_F}\right)^{-1} \cdot |h_{l_i}|^{-2}}}}\right).
\end{aligned}
\tag{3.41}
$$

3.4 Simulation Results

Both simulation and semi-analytical results are presented in this section. Each data symbol is transmitted over 8 or 16 sub-carriers ($N_F = 8$ or 16), and the time domain spreading factor is $N_T = 8$. Since we are interested in the case without MCI, the number of multiplexed frames $K = 8$ in order to maximize the transmission rate under the condition of no MCI. We assume CSI is perfectly known at the receiver side, and the channel is fixed for the duration of N_T OFCDM symbols. We simulate the system under Rayleigh fading and Ricean fading channels. All the curves of semi-analytical results are generated from Monte Carlo approach, where the BER expression are averaged over 100000 channel realizations.

Figure 3.5 shows the performance of a SISO-OFCDM system over Rayleigh fading channel with MRC. The frequency domain spreading factor is $N_F = 8$, and the sub-

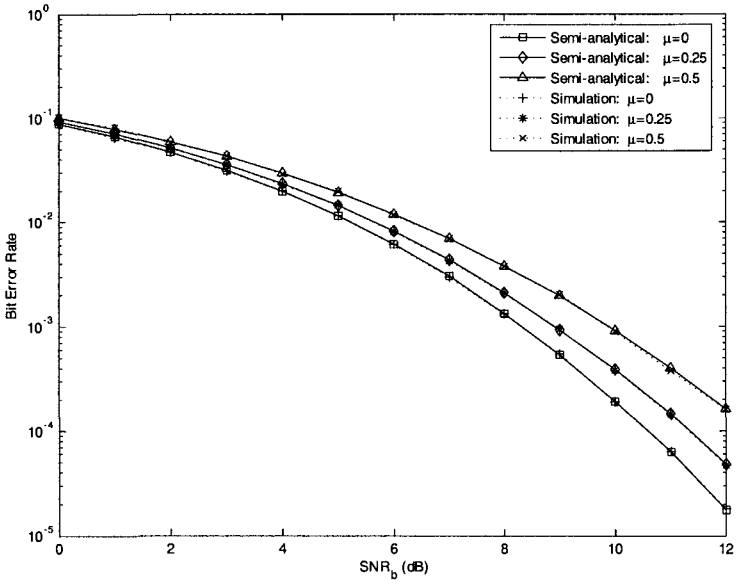

Figure 3.5: BER for SISO-OFCDM system using MRC over Rayleigh fading channel: $N_F = 8$, $N_T = 8$, $K = 8$

carriers of interest are separated enough to minimize the effect of correlation. Also simulation results are provided when the sub-carriers carrying the same information have correlation coefficients of 0, 0.25, and 0.5. From this figure we can see that the analytical results agree with the simulated ones. It is to be noted that our results are valid for a general OFCDM system with any system parameters. From these results, one can also see the effect of correlation on the overall diversity order.

In Figure 3.6, we present the performance of a SISO-OFCDM system over Ricean fading channel. EGC is used to achieve frequency diversity. The frequency domain spreading factor is $N_F = 16$. Different values of κ (i.e. the ratio of dominant component to the total power of scattered waves) are used in modeling the Ricean channel. As a reference, we include the performance over Gaussian channel. From these results

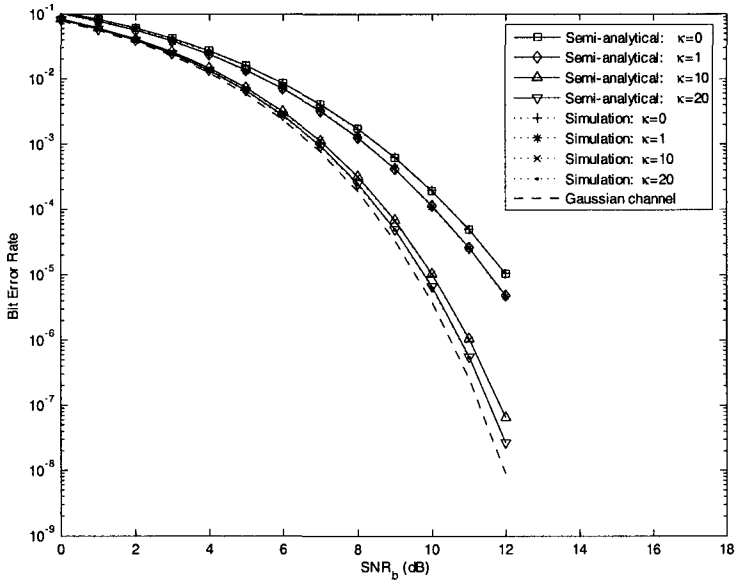

Figure 3.6: BER for SISO-OFCDM system using EGC over Ricean fading channel: $N_F = 16$, $N_T = 8$, $K = 8$

we can see the agreement between the analytical results and simulated ones.

Figure 3.7 presents the performance of a SISO-OFCDM system over Rayleigh fading channels using MMSE combining with $N_F = 16$. Different degree of correlation between adjacent sub-carriers transmitting the same information are simulated to show the effect of correlation along with the accuracy of our analytical results.

In Figures 3.8, 3.9 we compare the performance of MRC, EGC, and MMSE combining methods. Figure 3.8 shows the performance of SISO-OFCDM systems without MCI (i.e. the number of multiplexed frames does not exceed the time domain spreading factor). We can see that when there is no MCI, MRC achieves the best performance since it maximizes the output SNR. MMSE and EGC perform slightly worse than MRC, but they all achieve the same diversity gain. Figure 3.9 presents

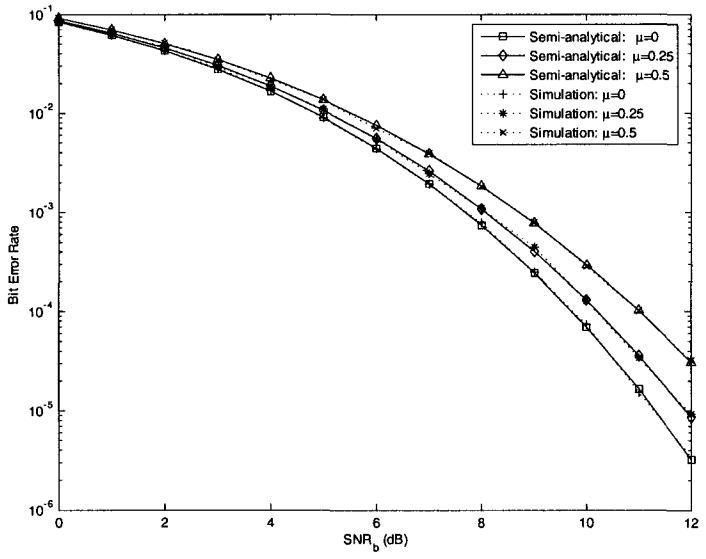

Figure 3.7: BER for SISO-OFCDM system using MMSE combining over Rayleigh fading channel: $N_F = 16$, $N_T = 8$, $K = 8$

the performance of a SISO-OFCDM system with MCI. In these results, the system is running at twenty-five percent of full load. Since the overall spreading factor $N_S = N_F \times N_T = 128$, from (3.2) one can see that twenty-five percent of full load implies that $K = 32$. In this system, every 4 symbols share the same time domain spreading code but with different frequency domain spreading codes. Hence, each transmitted symbol is interfered by other 3 symbols ($K_c = 3$). We can see that MMSE combining outperforms both MRC and EGC. This is due to the fact that among these three combining methods, MMSE combining is the only method that is adaptive, where MCI is accounted for during combining. It is clear that, only MMSE combining can achieve large diversity gains compared to MRC and EGC when MCI is present in the system.

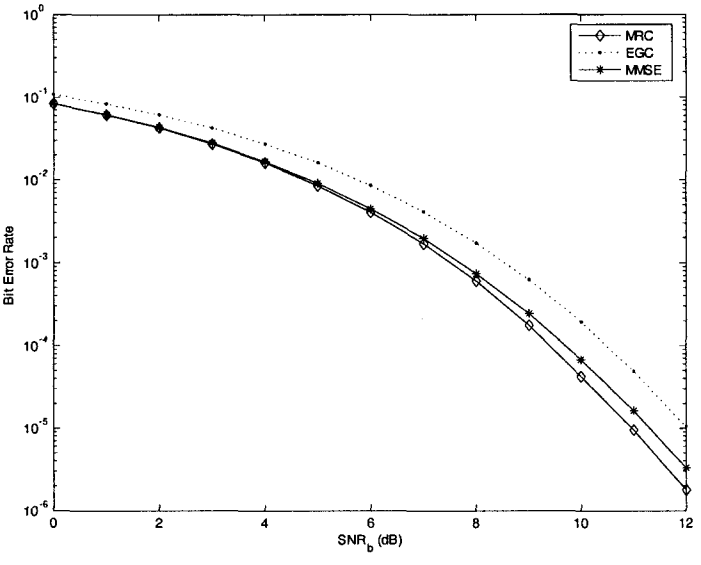

Figure 3.8: BER for SISO-OFCDM system without MCI over Rayleigh fading channel: $N_F = 16$, $N_T = 8$, $K = 8$

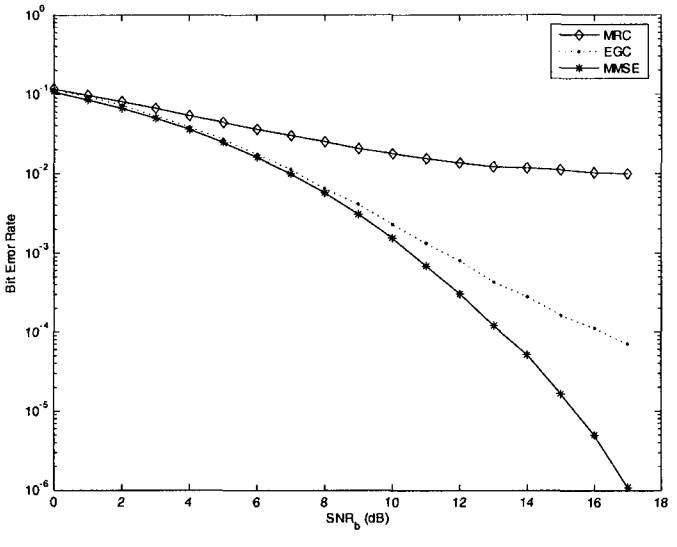

Figure 3.9: BER for SISO-OFCDM system with MCI over Rayleigh fading channel: $N_F = 16$, $N_T = 8$, $K = 32$

By comparing Figures 3.8 and 3.9, we can see the effect of MCI on system performance. The degradation of BER for MRC and EGC is clearly shown in Figure 3.9. When MMSE combining is employed, BER is less than 10^{-5} when SNR equals 12 dB in system with no MCI. In contrast, BER is greater than 10^{-4} at the same SNR when MCI is present. Therefore, a MCI cancellation scheme can be implemented to reduce this SNR loss.

3.5 Conclusion

In this chapter we have provided closed-form semi-analytical results for the BER of SISO-OFCDM systems without MCI. Our analytical results are proved to be accurate when compared with simulations. The performance of MRC, EGC, and MMSE combining techniques were compared in Ricean fading channels and Rayleigh fading as a special case. Also, we examined the effect of sub-carrier correlation and MCI on the system performance. Both simulation and analytical results proved that MMSE combining is optimal compared to both MRC and EGC when MCI is present.

CHAPTER 4

MIMO-OFCDM SYSTEMS

In the previous chapter, we studied SISO-OFCDM systems in terms of system structure, detection method, and their BER performance. In this chapter, we extend the results in chapter 3 to MIMO-OFCDM systems that employ STBC. Specifically, we study MIMO-OFCDM systems with two transmit and M receive antennas. Alamouti scheme is used to achieve transmit diversity, and gain combining techniques are used to extract receive diversity. The same as SISO-OFCDM systems, the performance of different combining schemes are studied for multiuser scenario, and BER semi-analytical results are then presented.

4.1 System Model

The transmitter structure of MIMO-OFCDM system is shown in Figure 4.1. In the MIMO-OFCDM system studied, the transmit diversity is achieved by hiring Alamouti scheme introduced in [1]. In order to implement Alamouti scheme, CSI is fixed over two frame duration, which is $2N_T$ times one OFCDM symbol duration. There are $N = 2$ transmit antennas and M receive antennas used in the MIMO-OFCDM system. At the beginning of each two frame duration, $2KN_B$ user data are modulated into BPSK symbols for transmission. Among these BPSK symbols, KN_B symbols are transmitted from the first transmit antenna, and the other KN_B sym-

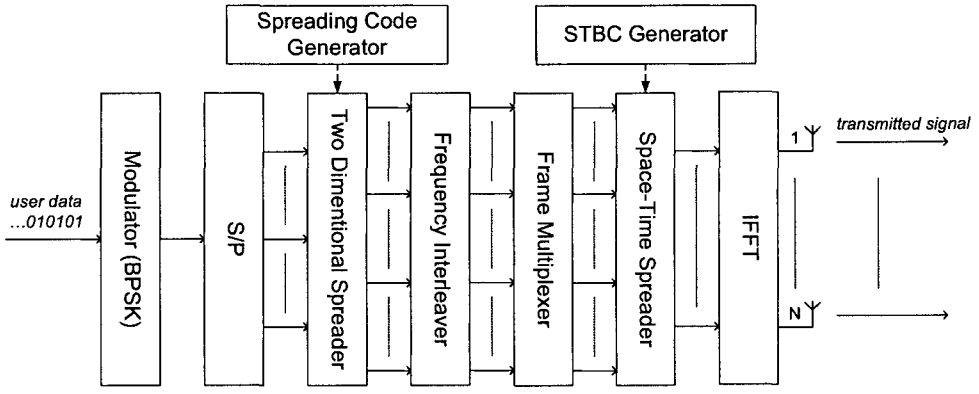

Figure 4.1: Transmitter structure of MIMO-OFCDM system

bols from the second transmit antenna. At each transmit antenna, the corresponding KN_B symbols are two-dimensionally spread and interleaved to form K frames, and these K frames are multiplexed into a super-frame.

Let the indices l_0,l_1,...,l_{N_F-1} represent the N_F sub-carriers carrying the k-th user data after frequency interleaving. Within the OFCDM super-frame transmitted from the n-th ($n = 1, 2$) transmit antenna, the transmitted signal on the l_i-th ($i = 0, 1, ..., N_F - 1$) sub-carrier during the j-th ($j = 0, 1, ..., N_T - 1$) OFCDM symbol duration is a summation of K OFCDM symbols and can be expressed as

$$S_n(l_i, j) = \sqrt{\frac{E_s}{2N_S}} \sum_{k=0}^{K-1} d_{n,k} c_{\lfloor \frac{l_i}{N_B} \rfloor N_T + j}(k), \tag{4.1}$$

where $d_{n,k}$ is the k-th user data that uses the l_i-th sub-carrier from the n-th transmit antenna in the first half of the two-frame duration, and $c_{\lfloor \frac{l_i}{N_B} \rfloor N_T + j}(k)$ is the $(\left\lfloor \frac{l_i}{N_B} \right\rfloor N_T + j)$-th chip of the k-th user's spreading code. We use S_1 and S_2 to represent the two super-frames at the two transmit antennas respectively. Then as shown in Figure 4.2, the OFCDM super-frames S_1, S_2, $-S_1^*$ and S_2^* are transmitted accord-

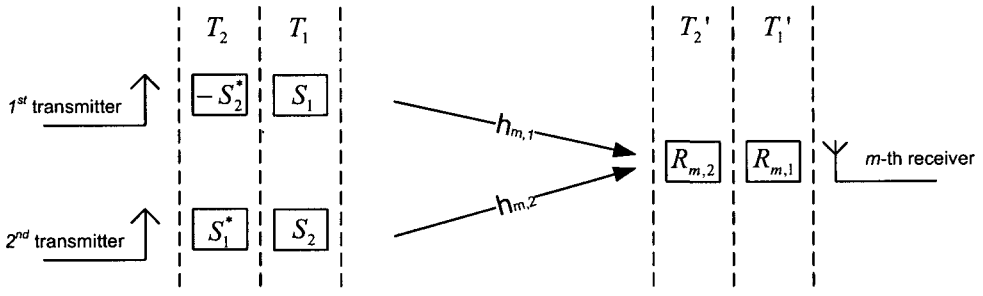

Figure 4.2: Alamouti scheme in MIMO OFCDM system

ing to Alamouti scheme through OFDM transmission system. During T_1, the first half of the two frame duration, S_1 is sent to the first transmit antenna and S_2 is sent to the second transmit antenna for transmission. During T_2, the second half of the two frame duration, S_2^* is sent to the first transmit antenna and $-S_1^*$ is sent to the second transmit antenna for transmission.

After experiencing channel fading and noise distortion, the signal is picked up by M receive antennas. Let us use $R_{m,1}$, $R_{m,2}$ to represent the received OFCDM super-frames for the two consecutive frame duration T_1' and T_2' at the receiver side shown in Figure 4.2. $R_{m,1}(l_i, j)$ and $R_{m,2}(l_i, j)$ represent the received OFCDM signal at m-th $(m = 1, 2, ..., M)$ receive antenna on the l_i-th sub-carrier during the j-th OFCDM symbol duration within the first and second frame duration respectively. We assume perfect synchronization. Therefore, $R_{m,1}(l_i, j)$ and $R_{m,2}(l_i, j)$ are given by

$$R_{m,1}(l_i, j) = \sqrt{\frac{E_s}{2N_S}} \sum_{k=0}^{K-1} \left(h_{l_i}^{m,1} d_{1,k} + h_{l_i}^{m,2} d_{2,k} \right) c_{\lfloor \frac{l_i}{N_B} \rfloor N_T + j}(k) + \eta_{m,1}(l_i, j) \qquad (4.2)$$

$$R_{m,2}(l_i, j) = \sqrt{\frac{E_s}{2N_S}} \sum_{k=0}^{K-1} \left(h_{l_i}^{m,1} d_{2,k}^* - h_{l_i}^{m,2} d_{1,k}^* \right) c_{\lfloor \frac{l_i}{N_B} \rfloor N_T + j}(k) + \eta_{m,2}(l_i, j), \qquad (4.3)$$

where $h_{l_i}^{m,n}$ $(m = 1, 2, ..., M,\ n = 1, 2)$ is the fading coefficient on the l_i-th sub-carrier

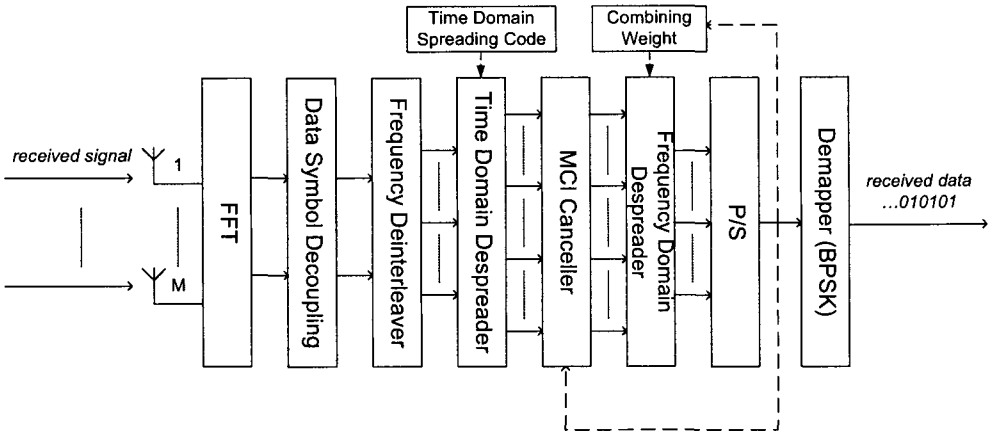

Figure 4.3: Receiver structure of MIMO-OFCDM system

from the n-th ($tr = 1, 2$) transmit antenna to the m-th receive antenna, $\eta_{m,1}(l_i, j)$ and $\eta_{m,2}(l_i, j)$ are the noise terms added to the signal on the l_i-th sub-carrier during the j-th OFCDM symbol duration at the m-th receive antenna.

4.2 Detection Algorithm

In this section, we propose the detection algorithm to recover the transmitted data symbols. This algorithm extracts receive diversity based on the optimal decision for Alamouti scheme with multiple receive antennas, which is given in (2.27) and (2.28). Figure 4.3 presents the receiver structure of MIMO-OFCDM system.

At the receiver side, each transmitted OFCDM symbol pair are decoupled over all receive antennas. These decoupled signals are then combined over all sub-carriers of interest to form the decision variables.

The transformed received signals, denoted as $\widetilde{Y}_1(l_i, j)$ and $\widetilde{Y}_2(l_i, j)$, at the l_i-th

sub-carrier within the j-th OFCDM symbol duration are given by

$$\begin{aligned}\widetilde{Y}_1(l_i,j) &= \sum_{m=1}^{M}\left[\left(h_{l_i}^{m,1}\right)^* R_{m,1}(l_i,j)+h_{l_i}^{m,2}\left[R_{m,2}(l_i,j)\right]^*\right] \\ &= \sqrt{\frac{E_s}{2N_S}}\sum_{k=0}^{K}\sum_{m=1}^{M}\left(\left|h_{l_i}^{m,1}\right|^2+\left|h_{l_i}^{m,2}\right|^2\right)d_{1,k}c_{\left\lfloor\frac{l_i}{N_B}\right\rfloor N_T+j}(k)+\eta_1^{eq}(l_i,j) \quad (4.4)\end{aligned}$$

$$\begin{aligned}\widetilde{Y}_2(l_i,j) &= \sum_{m=1}^{M}\left[\left(h_{l_i}^{m,2}\right)^* R_{m,1}(l_i,j)-h_{m}^{m,1}\left[R_{m,2}(l_i,j)\right]^*\right] \\ &= \sqrt{\frac{E_s}{2N_S}}\sum_{k=0}^{K}\sum_{m=1}^{M}\left(\left|h_{l_i}^{m,1}\right|^2+\left|h_{l_i}^{m,2}\right|^2\right)d_{2,k}c_{\left\lfloor\frac{l_i}{N_B}\right\rfloor N_T+j}(k)+\eta_2^{eq}(l_i,j), \quad (4.5)\end{aligned}$$

where the equivalent noise after combining becomes

$$\eta_1^{eq}(l_i,j)=\sum_{m=1}^{M}\left[\left(h_{l_i}^{m,1}\right)^*\cdot\eta_{m,1}(l_i,j)+h_{l_i}^{m,2}\cdot\left[\eta_{m,2}\left(l_i,j\right)\right]^*\right] \quad (4.6)$$

$$\eta_2^{eq}(l_i,j)=\sum_{m=1}^{M}\left[\left(h_{l_i}^{m,2}\right)^*\cdot\eta_{m,1}(l_i,j)-h_{l_i}^{m,1}\cdot\left[\eta_{m,2}\left(l_i,j\right)\right]^*\right]. \quad (4.7)$$

The equivalent channel parameters to on the l_i-th sub-carrier is given by

$$h_{l_i}^{eq}=\sum_{m=1}^{M}\left(\left|h_{l_i}^{m,1}\right|^2+\left|h_{l_i}^{m,2}\right|^2\right). \quad (4.8)$$

$\eta_1^{eq}(l_i,j)$ and $\eta_2^{eq}(l_i,j)$ are both Gaussian with zero mean and the variance

$$\begin{aligned}E\left\{\left|\eta_1^{eq}(l_i,j)\right|^2\right\} &= E\left\{\left|\eta_2^{eq}(l_i,j)\right|^2\right\} \\ &= \sum_{m=1}^{M}\left(\left|h_{l_i}^{m,1}\right|^2+\left|h_{l_i}^{m,2}\right|^2\right)E\left\{\left|\eta_{m,1}(l_i,j)\right|^2\right\} \\ &= \sum_{m=1}^{M}\left(\left|h_{l_i}^{m,1}\right|^2+\left|h_{l_i}^{m,2}\right|^2\right)E\left\{\left|\eta_{m,2}(l_i,j)\right|^2\right\} \\ &= \sum_{m=1}^{M}\left(\left|h_{l_i}^{m,1}\right|^2+\left|h_{l_i}^{m,2}\right|^2\right). \quad (4.9)\end{aligned}$$

The received signal transmitted from the n-th transmitting antenna during T_1 on the l_i-th sub-carrier using the K_T-th time domain spreading code, after time domain

despreading is given by

$$\begin{aligned} r_n(l_i) &= \frac{1}{N_T}\sum_{j=0}^{N_T-1}\widetilde{Y}_n(l_i,j)\times c_j^T(k) \\ &= \sqrt{\frac{E_s}{2N_S}}h_{l_i}^{eq}d_{n,k}c^F_{\left\lfloor\frac{l_i}{N_B}\right\rfloor}(k)+\overline{\eta}_n^{eq}(l_i). \end{aligned} \tag{4.10}$$

Then a suitable combining method is employed to extract frequency domain diversity over N_F sub-carriers of interest. The combining weight for the l_i-th sub-carrier is given below

- for MRC,

$$w^{eq}(l_i) = \left(h_{l_i}^{eq}\right)^* = h_{l_i}^{eq}, \tag{4.11}$$

- for EGC,

$$w^{eq}(l_i) = \frac{\left(h_{l_i}^{eq}\right)^*}{\left|h_{l_i}^{eq}\right|} = 1, \tag{4.12}$$

- for MMSE combining without MCI,

$$w^{eq}(l_i) = \frac{\left(h_{l_i}^{eq}\right)^*}{\left(h_{l_i}^{eq}\right)^2+\left(\frac{E_s}{2N_FN_0}\right)^{-1}} = \frac{h_{l_i}^{eq}}{\left(h_{l_i}^{eq}\right)^2+\left(\frac{E_s}{2N_FN_0}\right)^{-1}}. \tag{4.13}$$

The output of the frequency domain despreader is given by

$$y_{n,k} = \sum_{i=0}^{N_F-1} r_n(l_i)\cdot c^F_{\left\lfloor\frac{l_i}{N_B}\right\rfloor}(k)\cdot w^{eq}(l_i). \tag{4.14}$$

Then this output is normalized to form the decision variable, which will be used in MCI cancellation if needed. The decision variable is given by

$$z_{n,k} = \frac{1}{\sqrt{\frac{E_s}{2N_S}}}\cdot\frac{y_{n,k}}{\sum_{i=0}^{N_F-1}h_{l_i}^{eq}\cdot w^{eq}(l_i)}. \tag{4.15}$$

Finally a hard decision based on minimum distance criteria is made to recover the corresponding user data:

$$\widehat{d}_{n,k} = \arg\min_{\{s\}} |z_{n,k} - s|^2 , \tag{4.16}$$

where $\{s\}$ is the set of all possible transmitted data symbols.

4.3 Performance Evaluation

In this section, we derive the BER expression for MIMO-OFCDM systems using Alamouti scheme with multiple receive antennas for MRC, EGC, and MMSE combining.

Let $\overrightarrow{e_n}$ represent the error vector corresponding to the data symbols sent to the n-th transmit antenna during T_1, then $\overrightarrow{e_n}$ is given by

$$\begin{aligned}
\overrightarrow{e_n} &= z_{n,k} - d_{n,k} \\
&= \frac{\sum_{i=0}^{N_F-1} r_n(l_i) \cdot c^F_{\left\lfloor \frac{l_i}{N_B} \right\rfloor}(k) \cdot w^{eq}(l_i)}{\sqrt{\frac{E_s}{2N_S}} \sum_{i=0}^{N_F-1} h^{eq}_{l_i} \cdot w^{eq}(l_i)} - d_{n,k} \\
&= \frac{\sum_{i=0}^{N_F-1} \overline{\overline{\eta}}^{eq}_n(l_i) \cdot w^{eq}(l_i)}{\sqrt{\frac{\widetilde{\rho}}{2N_S}} \sum_{i=0}^{N_F-1} h^{eq}_{l_i} \cdot w^{eq}(l_i)},
\end{aligned} \tag{4.17}$$

where $h^{eq}_{l_i}$ is given by (4.8), $\widetilde{\rho}$ is the ratio of total transmitted power of each data symbol during T_1 and T_2 to the background noise power, and $\overline{\overline{\eta}}^{eq}_n(l_i)$ is the equivalent noise of the l_i-th sub-carrier at the receiver side during T'_n $(n = 1, 2)$. Since the additive noise terms $\eta_{m,1}(l_i, j)$ and $\eta_{m,2}(l_i, j)$ are complex AWGN with 0.5 per dimension, it is easy to show that the equivalent noise, $\overline{\overline{\eta}}^{eq}_n(l_i)$, is complex Gaussian noise with zero mean and variance $\frac{1}{2N_T} \sum_{m=1}^{M} \left(\left| h^{m,1}_{l_i} \right|^2 + \left| h^{m,2}_{l_i} \right|^2 \right) = \frac{h^{eq}_{l_i}}{2N_T}$ per dimension.

Conditioned on the channel, $\sum_{i=0}^{N_F-1} \overline{\overline{\eta}}_n^{eq}(l_i) \cdot w^{eq}(l_i)$ is also Gaussian with zero mean and variance

$$\sigma_{\tilde{\eta}}^2 = \frac{1}{N_T} \sum_{i=0}^{N_F-1} h_{l_i}^{eq} \left| w^{eq}(l_i) \right|^2 . \tag{4.18}$$

4.3.1 MRC

With MRC, since the equivalent channel coefficient $h_{l_i}^{eq}$ is a real number,

$$w(l_i) = \left(h_{l_i}^{eq}\right)^* = h_{l_i}^{eq}. \tag{4.19}$$

The error vector $\overrightarrow{e_n}$ becomes

$$\overrightarrow{e_n} = \frac{\sum_{i=0}^{N_F-1} \overline{\overline{\eta}}_n^{eq}(l_i) \cdot w^{eq}(l_i)}{\sqrt{\frac{\tilde{\rho}}{2N_S}} \sum_{i=0}^{N_F-1} h_{l_i}^{eq} \cdot w^{eq}(l_i)} = \frac{\sum_{i=0}^{N_F-1} \overline{\overline{\eta}}_n^{eq}(l_i) \cdot h_{l_i}^{eq}}{\sqrt{\frac{\tilde{\rho}}{2N_S}} \sum_{i=0}^{N_F-1} \left(h_{l_i}^{eq}\right)^2}, \tag{4.20}$$

and

$$\sigma_{\tilde{\eta}}^2 = \frac{1}{N_T} \sum_{i=0}^{N_F-1} h_{l_i}^{eq} \left| w(l_i) \right|^2 = \frac{1}{N_T} \sum_{i=0}^{N_F-1} \left(h_{l_i}^{eq}\right)^3 . \tag{4.21}$$

When BPSK modulation is used, the probability of bit error conditioned on the channel is given by

$$\begin{aligned} BER|_h &= P\left(\mathrm{Re}(\overrightarrow{e_n}) > 1\right) \\ &= P\left(\mathrm{Re}\left(\frac{\sum_{i=0}^{N_F-1} \overline{\overline{\eta}}_n^{eq}(l_i) \cdot w^{eq}(l_i)}{\sqrt{\frac{\tilde{\rho}}{2N_S}} \sum_{i=0}^{N_F-1} h_{l_i}^{eq} \cdot w^{eq}(l_i)} \right) > 1 \right) \\ &= Q\left(\frac{\sqrt{\frac{\tilde{\rho}}{N_F}} \sum_{i=0}^{N_F-1} \left(h_{l_i}^{eq}\right)^2}{\sqrt{\sum_{i=0}^{N_F-1} \left(h_{l_i}^{eq}\right)^3}} \right). \end{aligned} \tag{4.22}$$

4.3.2 EGC

With EGC, the combining weight of each sub-carrier is:

$$w(l_i) = \frac{\left(h_{l_i}^{eq}\right)^*}{h_{l_i}^{eq}} = 1. \tag{4.23}$$

The error vector $\overrightarrow{e_n}$ becomes

$$\overrightarrow{e_n} = \frac{\sum_{i=0}^{N_F-1} \overline{\overline{\eta}}_n^{eq}(l_i) \cdot w^{eq}(l_i)}{\sqrt{\frac{\widetilde{\rho}}{2N_S}} \sum_{i=0}^{N_F-1} h_{l_i}^{eq} \cdot w^{eq}(l_i)} = \frac{\sum_{i=0}^{N_F-1} \overline{\overline{\eta}}_n^{eq}(l_i)}{\sqrt{\frac{\widetilde{\rho}}{2N_S}} \sum_{i=0}^{N_F-1} h_{l_i}^{eq}}, \tag{4.24}$$

and

$$\sigma_{\widetilde{\eta}}^2 = \frac{1}{N_T} \sum_{i=0}^{N_F-1} h_{l_i}^{eq} |w(l_i)|^2 = \frac{1}{N_T} \sum_{i=0}^{N_F-1} h_{l_i}^{eq}. \tag{4.25}$$

Therefore, the probability of bit error conditioned on the channel is given by

$$\begin{aligned} BER|_h &= P\left(\mathrm{Re}(\overrightarrow{e_{tr}}) > 1\right) \\ &= P\left(\mathrm{Re}\left(\frac{\sum_{i=0}^{N_F-1} \overline{\overline{\eta}}_n^{eq}(l_i)}{\sqrt{\frac{\widetilde{\rho}}{2N_S}} \sum_{i=0}^{N_F-1} h_{l_i}^{eq}}\right) > 1\right) \\ &= Q\left(\sqrt{\frac{\widetilde{\rho}}{N_F} \sum_{i=0}^{N_F-1} h_{l_i}^{eq}}\right). \end{aligned} \tag{4.26}$$

4.3.3 MMSE Combining

The combining weight of MMSE combining for the systems without MCI is

$$w(l_i) = \frac{\left(h_{l_i}^{eq}\right)^*}{\left(h_{l_i}^{eq}\right)^2 + \left(\frac{E_s}{2N_F N_0}\right)^{-1}} = \frac{h_{l_i}^{eq}}{\left(h_{l_i}^{eq}\right)^2 + \left(\frac{\widetilde{\rho}}{2N_F}\right)^{-1}}. \tag{4.27}$$

The error vector $\overrightarrow{e_n}$ is given by

$$\overrightarrow{e_n} = \frac{\sum_{i=0}^{N_F-1} \overline{\overline{\eta}}_n^{eq}(l_i) \cdot w^{eq}(l_i)}{\sqrt{\frac{\widetilde{\rho}}{2N_S}} \sum_{i=0}^{N_F-1} h_{l_i}^{eq} \cdot w^{eq}(l_i)} = \frac{\sum_{i=0}^{N_F-1} \overline{\overline{\eta}}_n^{eq}(l_i) \cdot \frac{h_{l_i}^{eq}}{\left(h_{l_i}^{eq}\right)^2 + \left(\frac{\widetilde{\rho}}{2N_F}\right)^{-1}}}{\sqrt{\frac{\widetilde{\rho}}{2N_S}} \sum_{i=0}^{N_F-1} \frac{\left(h_{l_i}^{eq}\right)^2}{\left(h_{l_i}^{eq}\right)^2 + \left(\frac{\widetilde{\rho}}{2N_F}\right)^{-1}}}, \tag{4.28}$$

and

$$\begin{aligned}\sigma_{\tilde{\eta}}^2 &= \frac{1}{N_T}\sum_{i=0}^{N_F-1} h_{l_i}^{eq}\left|w^{eq}(l_i)\right|^2 \\ &= \frac{1}{N_T}\sum_{i=0}^{N_F-1}\frac{\left(h_{l_i}^{eq}\right)^3}{\left[\left(h_{l_i}^{eq}\right)^2+\left(\frac{\tilde{\rho}}{2N_F}\right)^{-1}\right]^2}.\end{aligned} \tag{4.29}$$

Then, we can find the probability of bit error conditioned on the channel as

$$\begin{aligned}BER|_h &= P\left(\mathrm{Re}\left(\frac{\sum_{i=0}^{N_F-1}\overline{\eta}_n^{eq}(l_i)\cdot\frac{h_{l_i}^{eq}}{\left(h_{l_i}^{eq}\right)^2+\left(\frac{\tilde{\rho}}{2N_F}\right)^{-1}}}{\sqrt{\frac{\tilde{\rho}}{2N_S}}\sum_{i=0}^{N_F-1}\frac{\left(h_{l_i}^{eq}\right)^2}{\left(h_{l_i}^{eq}\right)^2+\left(\frac{\tilde{\rho}}{2N_F}\right)^{-1}}}\right)>1\right) \\ &= Q\left(\frac{\sqrt{2}\sum_{i=0}^{N_F-1}\frac{1}{1+\left(\frac{\tilde{\rho}}{2N_F}\right)^{-1}\left(h_{l_i}^{eq}\right)^{-2}}}{\sqrt{\sum_{i=0}^{N_F-1}\frac{h_{l_i}^{eq}}{\frac{\tilde{\rho}}{2N_F}\left(h_{l_i}^{eq}\right)^2+2+\left(\frac{\tilde{\rho}}{2N_F}\right)^{-1}\left(h_{l_i}^{eq}\right)^{-2}}}}\right).\end{aligned} \tag{4.30}$$

4.4 Simulation Results

The simulation and semi-analytical results for MIMO-OFCDM systems are presented in this section. CSI is assumed to be perfectly known at the receiver side, and it is fixed for the duration of two consecutive OFCDM frames. Different system parameters are used when investigating the performance with MRC, EGC and MMSE combining.

Figure 4.4 presents the performance of MIMO-OFCDM systems with different number of receive antennas over Rayleigh fading channels using MRC. The analytical result for SISO-OFCDM system with $N_F = 8$ is shown as a reference. From this figure we can see the slop of the curves increases as the spatial diversity of the system increases. The MIMO-OFCDM systems with 1, 2, and 3 receive antennas have overall diversity orders of 16, 32, and 48 respectively, whereas the SISO-OFCDM system has

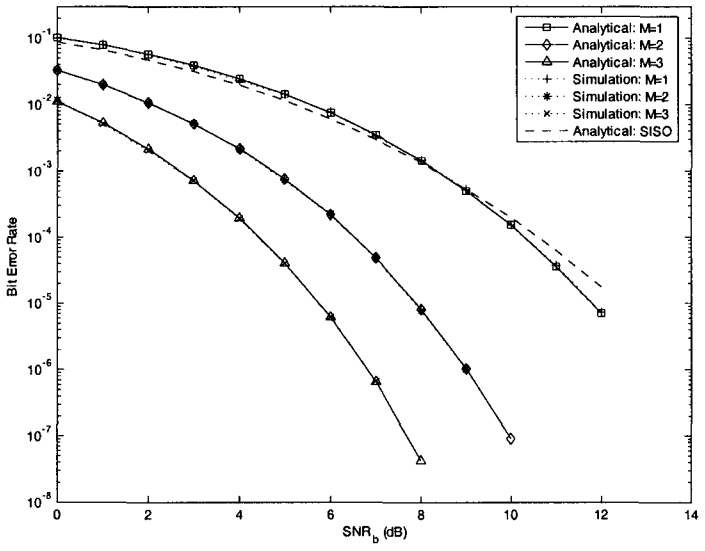

Figure 4.4: BER for MIMO-OFCDM system using MRC over Rayleigh fading channel: $N_F = 8$, $N_T = 8$, $K = 8$

a diversity order of 8. At the same time, we can see the accuracy of our semi-analytical results when compared with simulations.

In Figure 4.5 we investigate the performance degradation caused by correlation among sub-carriers of interest. The MIMO-OFCDM system employs two transmit antennas and two receive antennas with EGC. From this figure we can see that for SISO and MIMO-OFCDM systems, the impact on the overall diversity order is the same when sub-carriers of interest have correlation. This is because the correlation is only present among sub-carriers from the same transmit antenna to the same receive antenna. If spatial correlation exists in the MIMO system in addition to the correlation in frequency domain, the system performance will be degraded further.

Figure 4.6 shows the performance of MIMO-OFCDM systems over Rayleigh fading channels when MCI is introduced. The BER performance using different com-

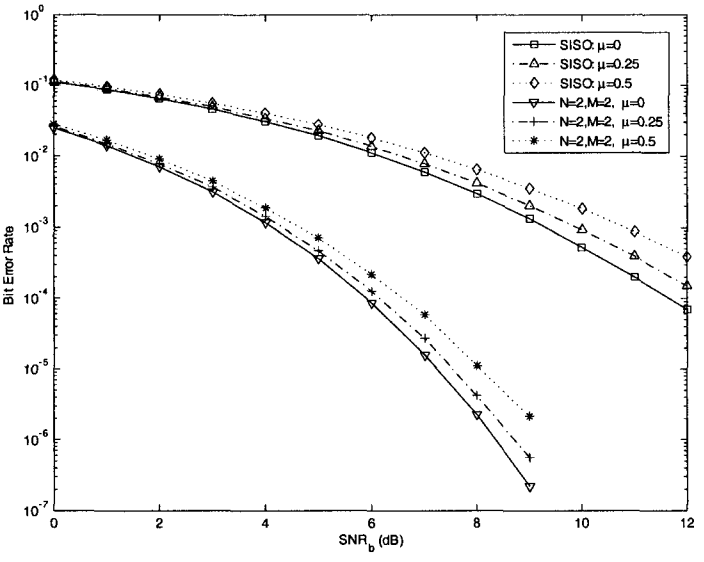

Figure 4.5: BER for OFCDM system using EGC over Rayleigh fading channel: $N_F = 8$, $N_T = 8$, $K = 8$

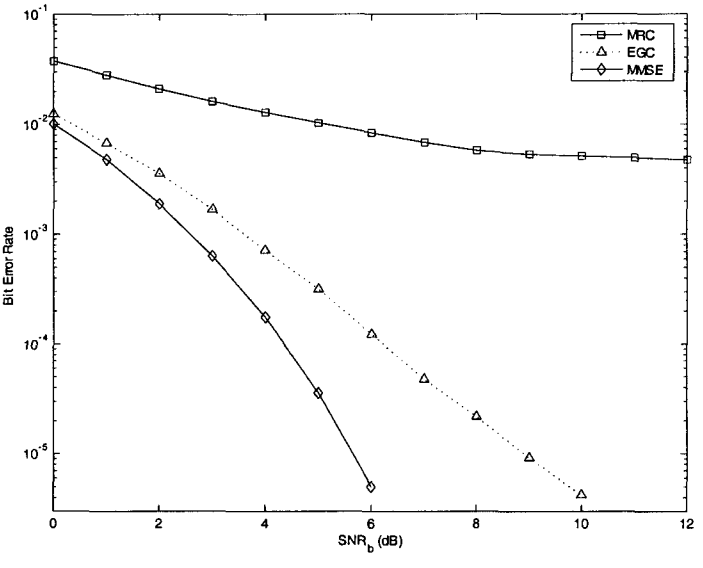

Figure 4.6: BER for MIMO-OFCDM system with MCI over Rayleigh fading channel: $N_F = 16$, $N_T = 8$, $N = 2$, $M = 3$, $K = 32$

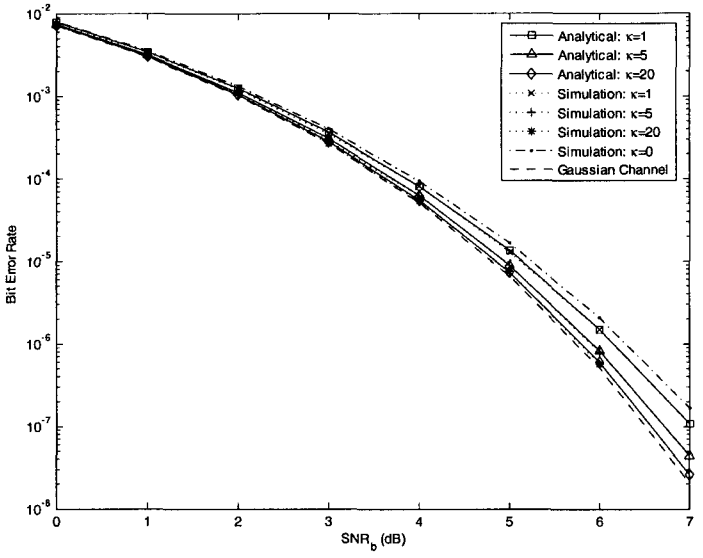

Figure 4.7: BER for MIMO-OFCDM system using EGC over Ricean fading channel: $M = 3$, $N_F = 8$, $N_T = 8$, $K = 8$

bining methods are compared. The results are presented for systems running at twenty-five percent of full load; that is every four spreading codes are interfering with each other. From this figure we can see that MMSE combining offers the best performance where it can deliver large diversity gain when MCI is present.

We present the performance of two MIMO-OFCDM systems over Ricean fading channels in Figs. 4.7 and 4.8, where three receive antennas with EGC and one receive antenna with MMSE combining are used in the two systems respectively. As a reference, we also present system performance over Gaussian channels with the same number of receive antennas. Systems with different values of κ are compared in both figures, where κ represents the ratio of the dominant component to the total power of scattered waves in Ricean fading channels. From these two figures we verified

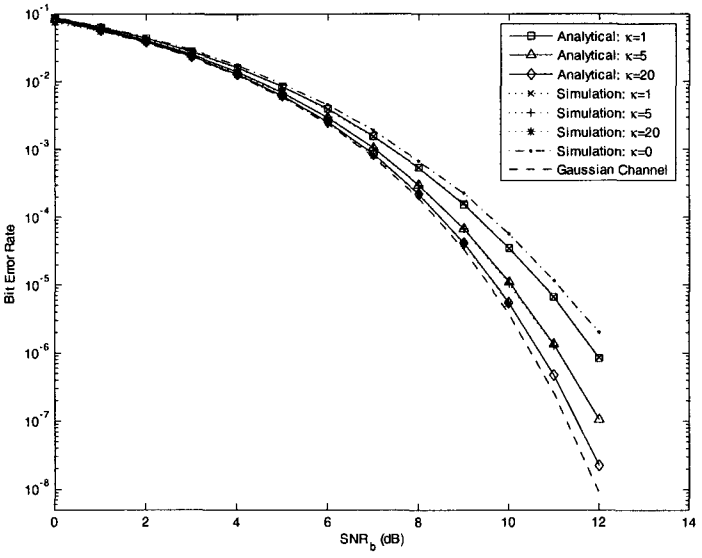

Figure 4.8: BER for MIMO-OFCDM system using MMSE combining over Ricean fading channel: $M = 1$, $N_F = 8$, $N_T = 8$, $K = 8$

that as κ increases from zero to infinity, the system performance converges to the performance on the Gaussian channel.

4.5 Conclusion

In this chapter we explained the transmission and detection methods for MIMO-OFCDM systems using Alamouti scheme with M receive antennas. It was shown that by employing STBC, MIMO-OFCDM systems provide significantly better performance than SISO-OFCDM systems without affecting the system transmission rate. We also derived BER semi-analytical results for MIMO-OFCDM with MRC, EGC, and MMSE combining methods. The analytical results obtained in this chapter are shown to be accurate when compared with the simulated ones. In addition, More-

over, we compared different combining methods when MCI is present, from which we showed that MMSE combining outperforms both MRC and EGC. Same as in the SISO-OFCDM cases, the analytical results we have obtained in this chapter are also applicable for general MIMO-OFCDM systems with different parameters over different fading channels.

CHAPTER 5

CONCLUSIONS AND FUTURE WORKS

5.1 Conclusions

In this section, we present a summary of the study accomplished in this thesis.

In Chapter 3, we studied the system structure, transmission and detection method, and the performance of SISO-OFCDM systems in downlink transmission. The SISO-OFCDM systems studied in this thesis involve two dimensional spreading in both time and frequency domains. At the receiver side, MRC, EGC, and MMSE combining techniques are employed to extract diversity in frequency domain. Semi-analytical expressions conditioned on the channel are derived for MRC, EGC, and MMSE combining in systems with no MCI. The accuracy of the semi-analytical results are proved by comparison with the simulated ones. Also, we examined the effects of sub-carrier correlation and MCI on the system BER.

In Chapter 4, we extended the results in Chapter 3 to MIMO-OFCDM systems when using STBC. By hiring Alamouti scheme with M receive antennas, we explained the signal structure, transmission and detection methods in MIMO-OFCDM systems. By implementing STBC, MIMO-OFCDM systems achieve spatial diversity on top of the frequency diversity, which shows significant improvement on the BER performance compared to SISO-OFCDM systems. Moreover, we derived the semi-analytical expressions of BER for different combining schemes in systems without

MCI. In addition, we checked the effect of sub-carrier correlation and MCI. The sub-carrier correlation has similar effect for both SISO and MIMO-OFCDM systems, and we confirmed MMSE combining is optimal when MCI is present in both SISO and MIMO-OFCDM systems.

5.2 Future Works

There are some future works that can be extended from this thesis.

1. We have derived the semi-analytical expressions for both SISO and MIMO-OFCDM systems. However, these expressions are conditioned on the channels. When the distribution of the channel coefficient is known, closed-form analytical results may be obtained.

2. In our study, we focused on systems without MCI. As mentioned in Chapter 3, we can approximate MCI as a Gaussian noise only when $K_c > 50$. However, how to include MCI in the semi-analytical expressions when $N_F < 50$ can be another extension of our study.

3. All the systems studied in this thesis assume downlink transmission, where the user data are perfectly synchronized. Therefore, the performance of up-link OFCDM transmission is also another interesting topic.

Bibliography

[1] S. M. Alamouti, "*A Simple Transmit Diversity Technique for Wireless Communications*," IEEE Journal Select. Areas Communications, Vol. 16, No. 8, pp. 1451-1458, October 1998.

[2] Tolga M. Duman and Ali Ghrayeb, *Coding for MIMO Communication Systems*, Wiley, 2007.

[3] V. Tarokh, N. Seshadri and A.R. Calderbank, "*Space-time Codes for High Data Rate Wireless Communication: Performance Criterion and Code Construction*," IEEE Transactions on Information Theory, Vol. 44, No. 2, pp. 744-765, March 1998.

[4] V. Tarokh, H. Jafarkhani and A.R. Calderbank, "*Space-time Block Coding for Wireless Communications: Performance Results*," IEEE Journal on Selected Areas in Communications, Vol. 17, No. 3, pp. 451-460, March 1999.

[5] Claude Oestges and Bruno Clerchx, *MIMO Wireless Communications: From Real-world Propagation to Space-time Code Design*, Academic Press, 2007.

[6] Gordon L. Stuber, *Principles of Mobile Communication*, Kluwer Academic Publishers, 2001.

[7] Leon W. Couch, II, *Digital and Analog Communication Systems*, Pearson, 2007.

[8] Rudolf Tanner, Jason Woodard, *WCDMA Requirements and Practical Design*, Wiley, 2004.

[9] Yiqing Zhou, Jiangzhou Wang, and Mamoru Sawahashi, "*Downlink Transmission of Broadband OFCDM System - Part I: Hybrid Detection*," IEEE Transaction on Communications, Vol. 53, No. 4, pp. 718-729, April 2005.

[10] Stefan Kaiser, "On the Performance of Different Detection Technique for OFDM-CDMA in Fading Channels," IEEE Global Telecommunications Conference 1995, Singapore, Vol. 3, pp. 2059-2063, 13-17 November 1995.

[11] Khairy El-Barbary and Hamed M. Alneyadi, "Comparison of the Behavior of MMSE Detection Scheme for DS-CDM and MC-CDMA," Second International Federation for Information Processing (IFIP) International Conference on Wireless and Optical Communications Networks, 2005, Dubai, United Arab Emirates, pp. 490 - 495, 6-8 March 2005.

[12] Stefan Kaiser, "Analytical Performance Evaluation of OFDM-CDMA Mobile Radio Systems," in Proc. First European Personal and Mobile Communication Conference (EPMCC'95), Bologna, Italy, pp. 215-220, November 1995.

[13] Yiqing Zhou, Tung-Sang Ng, Jiangzhou Wang, Higuchi K., Mamoru Sawahashi, "*OFCDM: A Promising Broadband Wireless Access Technique*," IEEE Communications Magazine, Vol. 46, No. 3, pp. 38-49, March 2008.

[14] J. G. Proakis, *Digital Communications*, Fourth Edition, McGraw Hill, 2000.

[15] Michel Daoud Yacoub, "The $\kappa-\mu$ Distribution: A General Fading Distribution," Vehicular Technology Conference, 2001 Fall, IEEE Vehicular Technology Society 54th, Atlantic City, NJ , USA, Vol. 3, pp. 1427-1431, 7-11 October 2001.

[16] Richard B. Ertel and Jeffrey H. Reed, "Generation of Two Equal Power Correlated Rayleigh Fading Envelopes," IEEE Communications Letters, Vol. 2, No. 10, pp. 276-278, October 1998.

[17] Charan Langton, "Orthogonal Frequency Division Multiplex (OFDM) Tutorial," Intuitive Guide to Principles of Communications, 2004.

[18] Patrick Robertson, Stefan Kaiser, "Analysis of the Loss of Orthogonality through Doppler Spread in OFDM Systems," Global Telecommunications Conference 1999, Rio de Janeiro, Brazil, Vol. 1B, pp. 701-706, December 1999.

[19] Tiejun (Ronald) Wang, John G. Proakis, and James R. Zeidler, "Techniques for Suppression of Intercarrier Interference in OFDM Systems," IEEE Wireless Communications and Networking Conference 2005, New Orleans, USA, Vol. 1, pp. 39-44, 13-17 March 2005.

[20] Kyeongcheol Yang and Seok-Il Chang, "Peak-to-average Power Control in OFDM Using Standard Arrays of Linear Block Codes," IEEE Communications Letters, Vol. 7, No. 4, pp. 174-176, April 2003.

[21] Haris Gacanin and Fumiyuki Adachi, "A Comprehensive Performance Comparison of OFDM/TDM Using MMSE-FDE and Conventional OFDM," IEEE Ve-

hicular Technology Conference, Spring 2008, Singapore, pp. 1404-1408, 11-14 May 2008.

[22] Zhe Wang and Yeheskel Bar-Ness, "Peak-to-Average Power Ratio Reduction by Polyphase Interleaving and Inversion for SFBC MIMO-OFDM with Generalized Complex Orthogonal Code," 40th Annual Conference on Information Sciences and Systems, 2006, Princeton, New Jersey, USA, pp. 317-320, 22-24 March 2006.

[23] Basel Rihawi, Yves Louet and Sidkieta Zabre, "PAPR Reduction Scheme with SOCP for MIMO-OFDM," International Conference on Wireless Communications, Networking and Mobile Computing, 2007, WiCom 2007, Shanghai, China, pp. 271-274, 21-25 September 2007.

[24] Mizhou Tan, Zoran Latinovie, and Yeheskel Bar-Ness, "STBC MIMO-OFDM Peak-to-Average Power Ratio Reduction by Cross-Antenna Rotation and Inversion," IEEE Communications Letters, Vol. 9, No. 7, pp. 592-594, July 2005.

[25] Muthanna AI-Mahmoud and Michael D. Zoltowski, "Performance evaluation of Code-Spread OFDM with error control coding," IEEE Military Communications Conference 2008, MILCOM 2008, San Diego, California, USA, pp. 1-6, 16-19 November 2008.

[26] Char-Dir Chung, "*Spectrally Precoded OFDM*," IEEE Transactions on Communications, Vol. 54, No. 12, pp. 2173-2185, December 2006.

[27] Xiaodong Wang, "OFDM and Its Application to 4G," International Conference on Wireless and Optical Communications 2005, 14th Annual WOCC 2005, Newark, New Jersey, USA, pp. 69, 22-23 April 2005.

[28] Jiangzhou Wang, *High-speed Wireless Communications: Ultra-wideband, 3G Long-Term Evolution, and 4G Mobile Systems*, Cambridge University Press, 2008.

[29] Emanuele Bizzarri, Antonio S. Gallo and Giorgio M. Vitetta, "Adaptive Space-Time-Frequency Coding Schemes for MIMO OFDM," IEEE Global Telecommunications Conference 2004, GLOBECOM '04, Dallas, Texas, Vol. 2, pp. 933-937, 29 November - 3 December 2004.

[30] Lingyun Lu, Yang Xiao, Shujun Zhang, "MMSE Space-Time Multi-user Detection in MIMO-OFDM System," 9th International Conference on Signal Processing, 2008, ICSP 2008, Beijing, China, pp. 1884-1887, 26-29 October 2008.

[31] Sam P. Alex and Louay M. A. Jalloul, "*Performance Evaluation of MIMO in IEEE802.16e/WiMAX*," IEEE Journal of Selected Topics in Signal Processing, Vol. 2, No. 2, pp. 181-190, April 2008.

[32] O.A. Alim, H.S. Abdallah and A.M. Elaskary, "Simulation of WiMAX System," IEEE Lebanon Communications Workshop 2008, LCW 2008, pp. 11-16, 31 May 2008.

[33] Zhengdong Luo, Junshi Liu, Ming Zhao, Yuanan Liu, and Jinchun Gao, "*Double-Orthogonal Coded Space-Time-Frequency Spreading CDMA Scheme*,"

IEEE Journal on selected areas in communications, Vol. 24, No. 6, pp. 1244-1255, June 2006.

[34] R. Wichman and A. Hottinen, "Multiuser Detection for Downlink CDMA Communications in Multipath Fading Channels," IEEE 47th Vehicular Technology Conference, 1997, Phoenix, Arizona, USA, Vol. 2, pp. 572-576, 4-7 May 1997.

[35] A. Catovic and S. Tekinay, "Selective Multiuser Detection for Cellular CDMA Systems," 12th IEEE International Symposium on Personal, Indoor and Mobile Radio Communications, 2001, San Diego, California, USA, Vol. 1, pp. D-17 - D-21, 30 September - 3 October 2001.

[36] "Multiuser Receiver Scheme for a Full-rate Space-time Block Coded CDMA System," International Conference on Communications, Circuits and Systems Proceedings 2006, Guilin, China, Vol. 2, pp. 948-952, 25-28 June 2006.

[37] S. Mohammad Razavizadeh, V. TabaTaba Vakili, P. Azmi and M. Fardis, "On Space-Time Block Coding in Downlink of Multiuser CDMA Systems," Proceedings of the Fifth IEEE International Symposium on Signal Processing and Information Technology, 2005, pp. 109-112, 21 December 2005.

[38] F. Horlin, E. Estraviz-Lopez and L. Van der Perre, "STBC for Uplink Single-carrier CDMA with Equalization in the Frequency Domain," IEEE Global Telecommunications Conference, 2005. GLOBECOM '05, St. Louis, MO, USA, Vol. 5, pp. 3154-3158, 2 December 2005.

[39] F. Petre, G. Leus, L. Deneire, M. Moonen, "Space-Time Coding for Single-Carrier Block-Spread CDMA Cellular Downlink," IEEE Global Telecommunications Conference, 2003, GLOBECOM '03, San Francisco, California, USA, Vol. 4, pp. 2345-2349, 1-5 December 2003.

[40] Noriyuki Maeda, Yoshihisa Kishiyama, Hiroyuki Atarashi, and Mamoru Sawashashi, "Variable Spreading Factor-OFCDM with Two Dimensional Spreading that Prioritizes Time Domain Spreading for Forward Link Broadband Wireless Access," Vehicular Technology Conference 2003, The 57th IEEE Semiannual, Jeju, Korea, Vol. 1, pp. 127-132, April 2003.

[41] S. Hara and R. Prasad, "*Overview of Multicarrier CDMA*," IEEE Communications Magazine, Vol. 35, No. 12, pp. 126-133, December 1997.

[42] A.C. McCormick and E.A. Al-Susa, "*Multicarrier CDMA for Future Generation Mobile Communication*," IEEE Electronics and Communication Engineering Journal, Vol. 14, No. 2, pp. 52-60, April 2002.

[43] V. M. Dasilva and E.S. Sousa, "Performance of Orthogonal CDMA Codes for Quasi-Synchronous Communication Systems," Proc. of IEEE International Conference on Universal Personal Communications, ICUPC '93, Ottawa, Canada, pp. 995-999, October 1993.

[44] Vincent Le Nir, Maryline HBlard and Rodolphe Le Gouable, "Space-Time Block Coding Applied to Turbo Coded Multicarrier CDMA," The 57th IEEE Semian-

nual Vehicular Technology Conference, VTC 2003-Spring, Jeju, Korea, Vol. 1, pp. 577-581, 22-25 April 2003.

[45] Zexian Li AND M. Latva-aho, "*Nonblind and Semiblind Space-Time-Frequency Multiuser Detection for Space-Time Block-Coded MC-CDMA*," IEEE Transactions on Wireless Communications, Vol. 4, No. 4, pp. 1311-1318 , July 2005.

[46] B. Golkar and F. Danilo-Lemoine, "Space-Time Coding and Spatial Multiplexing in MIMO Multicarrier CDMA," IEEE 18th International Symposium on Personal, Indoor and Mobile Radio Communications, 2007, PIMRC 2007, Athens, Greece, pp. 1-5, 3-7 September 2007.

[47] Yiqing Zhou, Jiangzhou Wang, and Mamoru Sawahashi, "*Downlink Transmission of Broadband OFCDM Systems - Part II: Effect of Doppler Shift*," IEEE Transactions on Communications, Vol. 54, No. 6, pp. 1097-1108, June 2006.

[48] S. Boumard, M. Weissenfelt, Huageng Chi and J. Nurmi, "A Wireless MIMO STC OFDM System Implementation," IEEE 17th International Symposium on Personal, Indoor and Mobile Radio Communications, pp. 1-5, 11-14 September 2006.

[49] M.Z. Win, J.H. Winters, "*Analysis of Hybrid Selection/Maximal-Ratio Combining in Rayleigh Fading*," IEEE Transactions on Communications, Vol. 47, No. 12, pp. 1773-1776, December 1999.

[50] Shinjiro Oshita, Norihiko Morinaga, Toshihiko Namekawa, "*Output Signal-to-Noise Ratio for Amplitude and Intensity Modulated Laser*", IEEE Transactions

on Aerospace and Electronic Systems, Vol. AES-10, No. 3, pp. 330-338, May 1974.

[51] George K. Karagiannidis, Dimitris A. Zogas, and Stavros A. Kotsopoulos, "*Statistical Properties of the EGC Output SNR Over Correlated Nakagame-m Fading Channels*," IEEE Transactions on Wireless Communications, Vol. 3, No. 5, pp. 1764-1769, September 2004.